NAVAL POSTGRADUATE SCHOOL
Monterey, California

THESIS

ADVANCEMENTS IN BURIED MINE DETECTION USING SEISMIC SONAR

by

Kraig E. Sheetz

December 2000

Thesis Advisor: Thomas G. Muir
Second Reader: Steven R. Baker

Approved for public release; distribution is unlimited

REPORT DOCUMENTATION PAGE		Form Approved OMB No. 0704-0188

Public reporting burden for this collection of information is estimated to average 1 hour per response, including the time for reviewing instruction, searching existing data sources, gathering and maintaining the data needed, and completing and reviewing the collection of information. Send comments regarding this burden estimate or any other aspect of this collection of information, including suggestions for reducing this burden, to Washington headquarters Services, Directorate for Information Operations and Reports, 1215 Jefferson Davis Highway, Suite 1204, Arlington, VA 22202-4302, and to the Office of Management and Budget, Paperwork Reduction Project (0704-0188) Washington DC 20503.

1. AGENCY USE ONLY *(Leave blank)*	2. REPORT DATE December 2000	3. REPORT TYPE AND DATES COVERED Master's Thesis

4. TITLE AND SUBTITLE: Title (Mix case letters) Advancements in Buried Mine Detection Using Seismic Sonar	5. FUNDING NUMBERS
6. AUTHOR(S) Kraig E. Sheetz	
7. PERFORMING ORGANIZATION NAME(S) AND ADDRESS(ES) Naval Postgraduate School Monterey, CA 93943-5000	8. PERFORMING ORGANIZATION REPORT NUMBER
9. SPONSORING / MONITORING AGENCY NAME(S) AND ADDRESS(ES) N/A	10. SPONSORING / MONITORING AGENCY REPORT NUMBER

11. SUPPLEMENTARY NOTES The views expressed in this thesis are those of the author and do not reflect the official policy or position of the Department of Defense or the U.S. Government.

12a. DISTRIBUTION / AVAILABILITY STATEMENT Approved for public release; distribution is unlimited	12b. DISTRIBUTION CODE

13. ABSTRACT *(maximum 200 words)*

Buried mines continue to disrupt the U.S. ability to project naval power ashore, conduct amphibious assaults, and wage land campaigns. This thesis describes advances in the development of a seismic sonar research tool that resulted in the successful detection of a Mk-63, 1000 lb, mine shape and a M-19, 20 lb, anti-tank mine. This seismic sonar research investigates the concept of using echo returns of a particular seismic interface wave, known as a Rayleigh wave, to detect buried mines. Rayleigh waves are unique in that they have elliptical particle motion that allows one to use vector polarization filtering to separate Rayleigh wave target reflections from other body waves with linear particle motion. A new source design employed in an array of seven elements has been shown to form a narrow beam of Rayleigh wave energy in a sand medium at the navy beach test site. This source beam, coupled with the receiver beam formed by an array of five three-component seismometers has provided a successful bi-static seismic sonar configuration. Signal to noise ratios of 21 dB for the Mk-63 mine shape, and 9 dB for the M-19 anti-tank mine were observed in the target echoes. These experimental results suggest that the seismic sonar is a very promising concept for buried mine detection.

14. SUBJECT TERMS Mine Warfare, Buried Mine Detection, Seismic Sonar, Surface Waves	15. NUMBER OF PAGES 98
	16. PRICE CODE

17. SECURITY CLASSIFICATION OF REPORT	18. SECURITY CLASSIFICATION OF THIS PAGE	19. SECURITY CLASSIFICATION OF ABSTRACT	20. LIMITATION OF ABSTRACT
Unclassified	Unclassified	Unclassified	UL

NSN 7540-01-280-5500

Standard Form 298 (Rev. 2-89)
Prescribed by ANSI Std. 239-18

THIS PAGE INTENTIONALLY LEFT BLANK

Approved for public release; distribution is unlimited

ADVANCEMENTS IN BURIED MINE DETECTION USING SEISMIC SONAR

Kraig E. Sheetz
Captain, United States Army
B.S., Millersville University, 1990
M.S., New Mexico Tech, 1992

Submitted in partial fulfillment of the
requirements for the degree of

MASTER OF SCIENCE IN APPLIED PHYSICS

from the

NAVAL POSTGRADUATE SCHOOL
December 2000

Author: _____
Kraig E. Sheetz

Approved by: _____
Thomas G. Muir, Thesis Advisor

_____
Steven R. Baker, Second Reader

_____
William B. Maier, Chairman
Department or Physics

THIS PAGE INTENTIONALLY LEFT BLANK

ABSTRACT

Buried mines continue to disrupt the U.S. ability to project naval power ashore, conduct amphibious assaults, and wage land campaigns. This thesis describes advances in the development of a seismic sonar research tool that resulted in the successful detection of a Mk-63, 1000 lb, mine shape and a M-19, 20 lb, anti-tank mine. This seismic sonar research investigates the concept of using echo returns of a particular seismic interface wave, known as a Rayleigh wave, to detect buried mines. Rayleigh waves are unique in that they have elliptical particle motion that allows one to use vector polarization filtering to separate Rayleigh wave target reflections from other body waves with linear particle motion. A new source design employed in an array of seven elements has been shown to form a narrow beam of Rayleigh wave energy in a sand medium at the navy beach test site. This source beam, coupled with the receiver beam formed by an array of five three-component seismometers has provided a successful bi-static seismic sonar configuration. Signal to noise ratios of 21 dB for the Mk-63 mine shape, and 9 dB for the M-19 anti-tank mine were observed in the target echoes. These experimental results suggest that the seismic sonar is a very promising concept for buried mine detection.

THIS PAGE INTENTIONALLY LEFT BLANK

TABLE OF CONTENTS

ACKNOWLEDGMENTS

This work was supported by the U.S. Navy Office of Naval Research, Codes 322W and 321OA, Drs. Douglas Todoroff, Jeffrey Simmen, and Edward Estalot, program manager. I am grateful to Professor Thomas Muir for his guidance and oversight of the project, and for his contagious passion for solving the buried mine problem. I would like to thank Professor Steven Baker for his valuable technical and data acquisition expertise. I owe great thanks to Mr. Don Snyder and Mr. George Jaksha of the NPS Physics Department for their design and engineering support for this project. The research tools would have never safely deployed to the field without their help. A thanks also goes to Jeremy Guy, the Co-Researcher on this project, whose dedication to the success of the project was paramount. Finally, I would like to thank my wife Lori, who provides never-ending support for all of my endeavors.

THIS PAGE INTENTIONALLY LEFT BLANK

I. INTRODUCTION

Since the U.S. Civil War, the use of land and sea mines has added a new dimension to all land and sea military operations. Buried mines and unexploded ordnance pose a serious threat to U.S. Military forces and civilian, non-combatant organizations around the world. This threat impedes U.S. abilities to project naval power ashore and conduct land war operations, while increasing the likelihood of casualties to American soldiers, sailors, and marines. During missions ranging from the conventional warfare of the Persian Gulf War, to the humanitarian relief mission in Somalia, and the peacekeeping/peacemaking missions in Bosnia and Kosovo, buried mines have represented a formidable force multiplier.

A. MILITARY RELEVENCE

1. The Naval Mine Problem

Detection of mines buried in shallow water is an increasingly important topic for U.S. Naval and Marine forces. The surf zone and very shallow water environments present a significant challenge for Mine Countermeasures (MCM) operations. The Gulf War illustrated the evolving nature of mine warfare and highlighted the requirement for MCM in shallow water. "...From the Sea" and "Forward...From the Sea" by the Chief of Naval Operations (1992 and 1994 respectively) emphasized the importance of warfare in littoral areas. [Ref. 1,2] In "Operational Maneuver from the Sea" (1996), the Commandant of the Marine Corps spelled out the operational concepts of maneuver warfare between sea and land, focusing of the requirement for rapid movement from ship to objective.[Ref. 3]

The projection of naval power ashore, including the effective delivery of U.S. amphibious forces, hinges on the ability to avoid and/or neutralize any possible mine threat. This is especially crucial in the vulnerable regions where amphibious forces transition from shallow water, through the surf zone, and onto the beach. Mines above the

seabed are typically capable of detection by sonar, and, to some extent, optical systems. However, once a mine is buried into a sand or silt bottom by wave or tidal action, the probability of detection declines dramatically. Naval mines like the "Manta" bottom mine scour below the surface and are buried due to water action. The threat of this elusive mine type is serious, as evidenced by the damage to the USS PRINCETON during Operation Desert Storm. A flexible, organic MCM capability to detect buried mines in the shallow water surf zone and on the beach is paramount to America's ability to successfully employ amphibious landing forces.

2. The Land Mine Problem

It is easy for U.S. adversaries to disrupt and even prevent land operations through the extensive use of land minefields. During the Gulf War, Iraqi minefields prevented U.S. Marines from establishing a beachhead, and they were a constant threat to coalition forces throughout the ground war. Over 300,000 land mines have been cleared from Kuwait since the war. Land mines killed several soldiers in Somalia during a mission initially thought to be simply humanitarian aide. Of all the threats facing U.S. soldiers in former Yugoslavia, land mines represent the gravest danger. Buried in the ground and strewn all over the land, anti-personnel mines killed one soldier and continue to threaten NATO peacekeeping forces there. In Tuzla, Bosnia, a team of four soldiers and airmen had to install and operate a navigational system to let mission essential aircraft land on a grass runway. The mud and bad weather provided formidable opposition to the mission, but the most serious obstacle was the threat of land mines. A Sergeant in charge of the operation stated "I wanted to know without a doubt that this area is clear...I didn't want anybody hurt". [Ref. 4]

While land mines clearly pose a threat to U.S. operations abroad, they are also an integral part of America's military doctrine. Asked about the U.S. position on the moratorium on using anti-personnel mines, pentagon spokesman Ken Bacon said the moratorium would "damage the ability of the military to carry out operations and protect troops." [Ref. 5] In Korea, some one million land mines are buried in the Demilitarized

Zone that divides North from South. Secretary of Defense William Cohen, on a visit to Korea, stated that "Without land mines, the capacity for the forces in the north would be certainly eased to roll through this area to downtown Seoul." [Ref. 6] The only alternative to those land mines is a substantially greater force structure on the peninsula, which places unacceptable risk on force structures supporting other theaters like the Persian Gulf and Bosnia.

It is vital that the U.S. develops technologies to build systems that can safely detect, classify, avoid and/or neutralize buried mines. Such systems must be as covert or clandestine as possible, and must be able to provide surveillance capabilities in non-hostile environments as well as "in-stride" mine detection during combat operations.

B. HUMANITARIAN IMPACTS

An estimated 100 million unexploded land mines left over from this century's various wars and conflicts lie scattered in 64 countries, and it is currently estimated that an additional five million new mines are placed in the ground each year. [Ref. 7] Many of these mines are of the anti-personnel variety which are designed to maim, rather than kill. They are chillingly effective for that purpose, each day claiming the limbs and lives of about 70 people, mostly civilians, in places like Cambodia, Angola, Ethiopia, Afghanistan, Bosnia, and other areas shown in Figure 1.1.

Land mines remain a relatively inexpensive and simple to manufacture weapon that is extremely effective both tactically and psychologically. Mine warfare is thus an attractive alternative for nations and rogue organizations that do not have the resources to develop sophisticated weapon systems. As a result, mine proliferation has become a worldwide problem with more than 49 countries possessing mining capabilities, and with 30 of these demonstrating mine production capabilities, and 20 of these attempting to export their mine warfare systems. [Ref. 8] Last year, mine-clearing operations around the world immobilized 120,000 devices; however, in the same period, about two and a half million landmines were manufactured. Even if the laying of land mines were to immediately grind to a halt today, the United Nations estimates that, with conventional

methods now being used, it would take over 1,000 years, at a cost of nearly $33 billion, to safely clear out the world's mine fields. [Ref. 7]

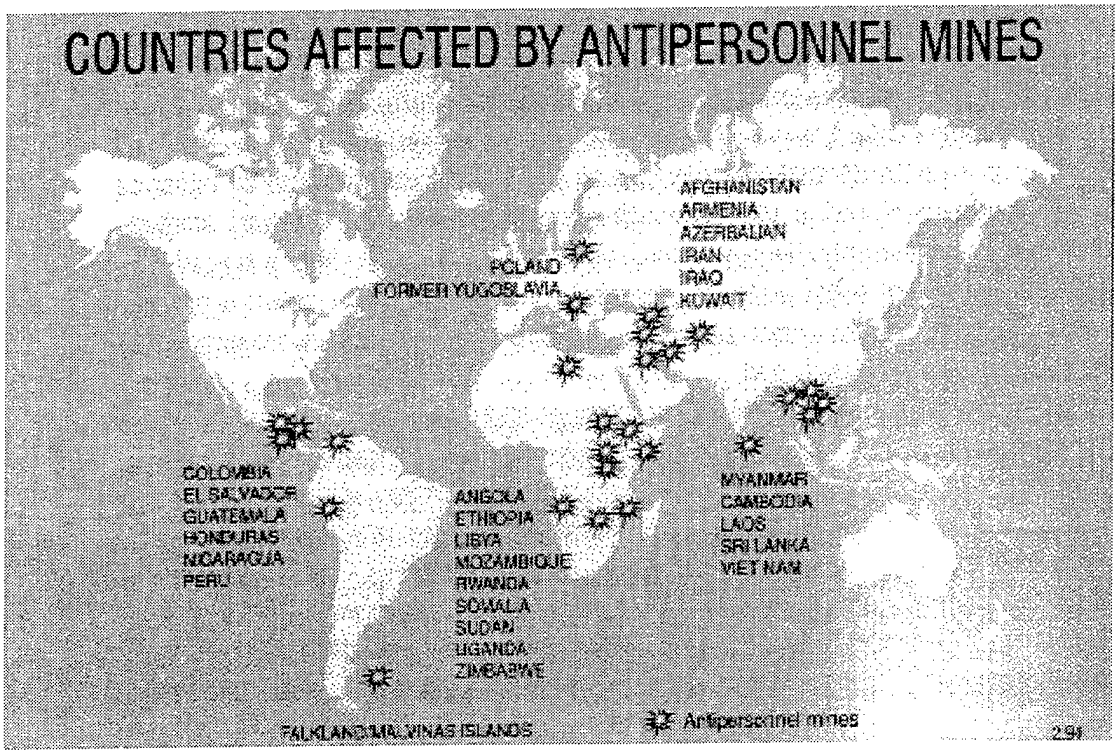

Figure 1.1. Countries laden with antipersonnel mines. From Ref. [7].

C. MINE DETECTION TECHNOLOGIES

There are a number of systems that can locate and sweep exposed mines and ordnance, however, detecting buried mines is a significantly more challenging problem. While some systems have limited success in specific environments, there is no single technology in existence that can detect buried mines in shallow water sediments, through the surf zone, and onto the beach and the solid ground beyond.

1. Current Technologies

The primary method used today for detecting buried mines on the beach and landward is hand probes and metal detectors. These methods, however, are very inefficient and dangerous and do not lend themselves to military operations. Additionally, almost all modern anti-personnel mines used today are relatively small, from about two inches to 20 inches in diameter, and are made of plastic with very few metal parts in them, making them very difficult to detect. [Ref. 7] Other methods that are currently available to detect buried mines are ground-penetrating radar and specially trained dogs that can sniff out explosives. The radar systems can detect non-metallic mines, but are very slow and must be operated directly over the mine at a very close distance (on the order of one foot). Such operations can thus be as dangerous as using metal detectors. Using explosive sniffing dogs poses serious logistical concerns for humanitarian de-mining and is simply not conducive to swift combat operations. In Somalia, mine reconnaissance operations were augmented with infrared cameras that had some success locating buried mines during certain times of the day. However, weather conditions and thick vegetation easily degraded the performance of these cameras.

With regard to buried naval mines, marine mammals are currently the only means the Navy has for detecting buried mines. The U.S. Navy's Marine Mammal Program incorporates specially trained Atlantic and Pacific Bottlenose Dolphins, (as well as white whales, and sea lions) for mine detection and neutralization. [Ref. 9] However, the mammals are cumbersome and expensive and cannot operate in the very shallow water of the surf zone.

2. New Technologies

There are a number of technologies currently being explored to take on the buried mine detection missions of the future. Some of the newer methods being tested involve technologies such as ground-penetrating radar, infrared emission, thermal neutron activation, and energetic photon detection. [Ref. 7] Some researchers are trying to

combine these new techniques with ordinary metal detectors to increase the discrimination (signal to noise, false target rejection, etc.), range, and search rate capabilities of their particular methods.

The Countermine Division of the Army's Project Manager for Mines, Countermine and Demolitions, located in Fort Belvoir, Virginia, is continuing to develop better ways to help field commanders detect, mark, and neutralize land mines. [Ref. 10] A current innovation is the Interim Vehicle-Mounted Mine Detector, which is a string of vehicles that moves at speeds up to nine miles per hour and is designed to detect, mark and detonate metallic anti-tank mines. This system, already used by the South African, French, and British armies, is currently being evaluated by the U.S. Army. The future version, called the Ground Standoff Minefield Detection System is due to be field tested in 2003, and is being designed to detect non-metallic mines as well. This system aims to employ several types of sensors to discriminate between mines and other field debris such as canteens, shell casings, and bayonets.

In 1998, the director of the Countermine Division, Mr. Brian Green, stated that even with all of the emerging technologies, there are "no silver bullets" that will guarantee 100 percent protection against the land mine threat. He stated that "It's important to recognize that in operations other than war, the threat is the same as during medium to high intensity conflicts...Our goal is to provide troops in the field the best technology available so that they can operate as safely and with as much confidence as possible."[Ref. 10]

This ideal is the motivation behind this thesis project where the concept of a seismic sonar system is developed one step further. The desired end state being a deployable system that can locate buried land and sea mines, in the littoral seas, the shallow surf zone, the beach, and onto the land battlefields and beyond.

D. RESEARCH OBJECTIVE

The purpose of this thesis is to present the results of developmental research on a seismic sonar. Based on initial research conducted by Applied Research Laboratories of

the University of Texas at Austin (ARL:UT) [Ref. 11], the seismic sonar is a research tool to detect buried mines and ordnance using seismic interface waves. The research of previous students at ARL:UT and the Naval Postgraduate School [Ref. 12,13,14] has shown promising results for the feasibility of using electromagnetic vibration sources to generate seismic interface, or surface waves. These surface waves then scatter from buried objects and can be used to detect, range, and determine the target strength of such objects. The objective of this research is to expand on the concept of the seismic sonar from individual sources and receivers to arrays of sources and receivers. This concept advancement provides two benefits. It utilizes the beam forming features of arrays and thus maximizes energy along a predetermined axis, and it allows for either mechanical or electronic steering of the beam axis. This thesis will focus on the development and testing of seismometer arrays and mechanical source arrays, as well as the overall configuration of the seismic sonar research tool. The goal of the research is to establish a configuration that will maximize the signal to noise ratio of surface waves scattered from buried mines and ordnance, and therefore maximize the seismic sonar detection range.

Once the concept of the seismic sonar is demonstrated, the capability can possibly evolve from a research tool to a "militarized" platform that is capable of detecting buried mines with real-time, on-board signal processing. This long-term goal requires a multi-disciplinary effort from physicists, mechanical and electrical engineers, mathematicians, and operations analysts in a cooperative effort to develop a new system to address the serious problem of buried mine detection.

THIS PAGE INTENTIONALLY LEFT BLANK

II. SEISMIC WAVES

Seismology is based on the theory of elasticity. The elastic properties of materials are characterized by their elastic moduli (or elastic constants), which specify the relation between stress and strain. The two moduli of interest for the study of elastic waves in the earth are the bulk modulus (k) and the shear modulus (μ). The bulk modulus is also referred to as the incompressibility and the shear modulus as the rigidity. Note that liquids and gases offer no resistance to shear deformation and thus have no shear modulus.

If the stress is suddenly applied to, or released from, an elastic medium, the condition of strain propagates within the medium as an elastic wave. There are several types of elastic waves which can be grouped into two categories, body waves and surface waves. In an infinite, homogeneous, solid, elastic, and isotropic medium, only body waves can propagate and the two types of body waves are called P-waves and S-waves. The term P-wave means "primary" waves because it travels faster and arrives first, and the S stands for "secondary" wave. If the medium is a homogeneous half-space (such as the earth with a free surface), then in addition to the body waves, there are surface waves with motion confined to the vicinity of the surface and decaying with depth. The following sections provide a brief overview of the characteristics of body waves and surface waves and highlights the features of surface waves that make them ideal tools to detect buried ordnance.

A. BODY WAVES

P-waves are longitudinal, or compressional, waves, and the motion of the medium is in the same direction as the wave propagation. The particle motion consists of alternating compressions and rarefactions during which adjacent particles of the solid are closer together and farther apart during successive half cycles. The compressional wave travels with velocity given by,

$$V_p = \sqrt{\frac{k + 4\mu/3}{\rho}}, \qquad (2.1)$$

where k is the bulk modulus, μ is the shear modulus and ρ is the density of the medium. Note that if the medium is liquid or gas, and μ=0, P-waves can still propagate.

In transverse or shear body waves (S-waves),the motion of the individual particles is perpendicular to the direction of wave propagation. The velocity of such waves is given by,

$$V_s = \sqrt{\frac{\mu}{\rho}}. \qquad (2.2)$$

Shear waves can be polarized in such a way that the particles oscillate within a definite plane perpendicular to the direction of wave propagation. These polarized waves are known as SH and SV waves in a geophysical context, with respect to the surface of the earth. A horizontally traveling shear wave polarized so that the particle motion is all vertical is designated as an SV wave; when its motion is all in the horizontal plane, it is called an SH wave. Note that pure body shear waves cannot propagate through liquids or gases (V_s=0).

B. INTERFACE WAVES

When "pure" body waves (P and S) impinge on a free surface of a solid, or on an interface with another medium, they are partly converted into each other, creating "mixed" wave types in the immediate vicinity of the interface. [Ref. 15] There are many different types of interface waves, some of which can occur at interfaces located deep within the earth's layered structure. However, this research focuses a subset of interface waves that are confined to the vicinity of the earth's surface. Because surface waves are confined near the surface, their energy spreads out only in two dimensions. On a half-space, these waves would spread out as circles; body waves, in contrast, would spread out

as half-spheres. Consequently, the amplitude of surface waves is proportional to the inverse of the square root of the distance, whereas the amplitude of body waves is inversely proportional to the distance.

A commonly known type is Rayleigh waves, which occur at the interface between a semi-infinite elastic half-space and a gas. They have both vertical and horizontal particle motion in a vertical plane oriented along the direction of propagation. In earthquakes, Rayleigh waves produce the destructive "ground roll" energy. Like gravity waves at sea, the motion of surface waves decays with depth. Another type of surface wave is the Scholte wave. Scholte waves have particle motion similar to Rayleigh waves, but occur at the interface between a liquid and an elastic half-space such as the seafloor. Surface waves that travel in a "channel" just beneath the surface are called ducted interface waves. The most common ducted wave is the Love wave, which propagates in a duct between two sedimentary boundaries. Love waves have particle motion that is horizontal and at right angles to the direction of propagation.

On the earth's surface, these and many other subsets of these types of surface waves can propagate. This research is conducted on a beach where the air-sand interface provides a condition for the propagation of both Rayleigh waves and Loves waves. Figure 2.1 shows how the characteristics of these two types of surface waves differ. Note that Scholte waves along a liquid-sediment interface (the sea floor) have the same characteristics as the Rayleigh waves in the figure.

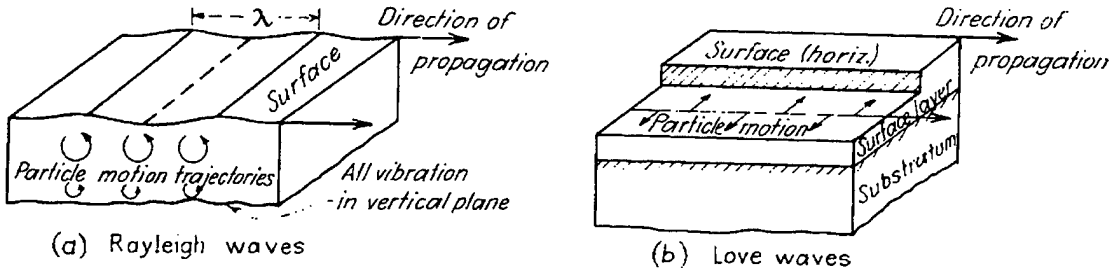

Figure 2.1. Characteristics of (a) Rayleigh Waves, and (b) Love Waves Traveling along the Surface of a Solid. From Ref. [16].

1. Rayleigh Waves

Lord Rayleigh demonstrated the existence of Rayleigh waves in 1887. These waves can propagate at the surface of a homogeneous solid or of a solid in which the velocity shows a general increase with depth. Applying the stress-free boundary condition (at the surface) to the elastic wave equation yields the Rayleigh wave equations given by

$$\frac{\partial^2 \phi}{dt^2} = V_p{}^2 \nabla^2 \phi \quad and \quad \frac{\partial^2 \Psi}{dt^2} = V_s{}^2 \nabla^2 \Psi, \qquad 2.3$$

where ϕ and ψ and the potential functions representing compression (P) and rotation (S) effects respectively. It can be shown that, for elastic solids, it is possible for a coupled pair of inhomogeneous waves, P and SV, to propagate along the surface of the half-space. [Ref. 17]

In Rayleigh wave motion, the paths of the particles of the medium are ellipses whose major axes are vertical and minor axes are in the direction of propagation of the wave. Figure 2.2 shows the two possible polarities for this elliptical motion. At the free surface, Rayleigh wave particle motion is elliptical and retrograde (having rolling motion opposite to the direction of propagation). Below a certain depth, which depends on wavelength, the particle motion becomes elliptical prograde (having rolling motion in the same direction as the propagation). Figure 2.3 shows a plot of vertical and horizontal particle motion as a function of depth. The depth h, at which the particle rotation direction shifts, occurs at approximately $0.1\lambda_R$, where λ_R is the Rayleigh wavelength. [Ref. 18]. Additionally, the particle motion is localized to a layer that is $2.0\lambda_R$ deep. Rayleigh waves propagate at roughly 0.9% of the shear wave velocity V_s.

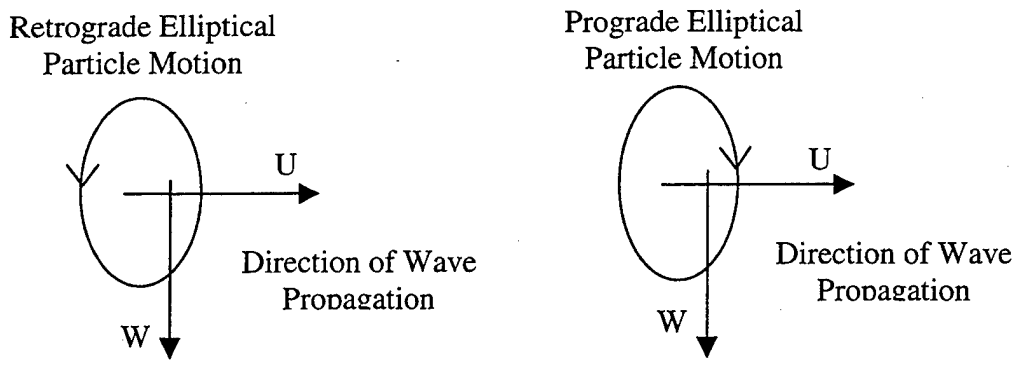

Figure 2.2. Rayleigh wave particle motion. U and W are horizontal and vertical displacement.

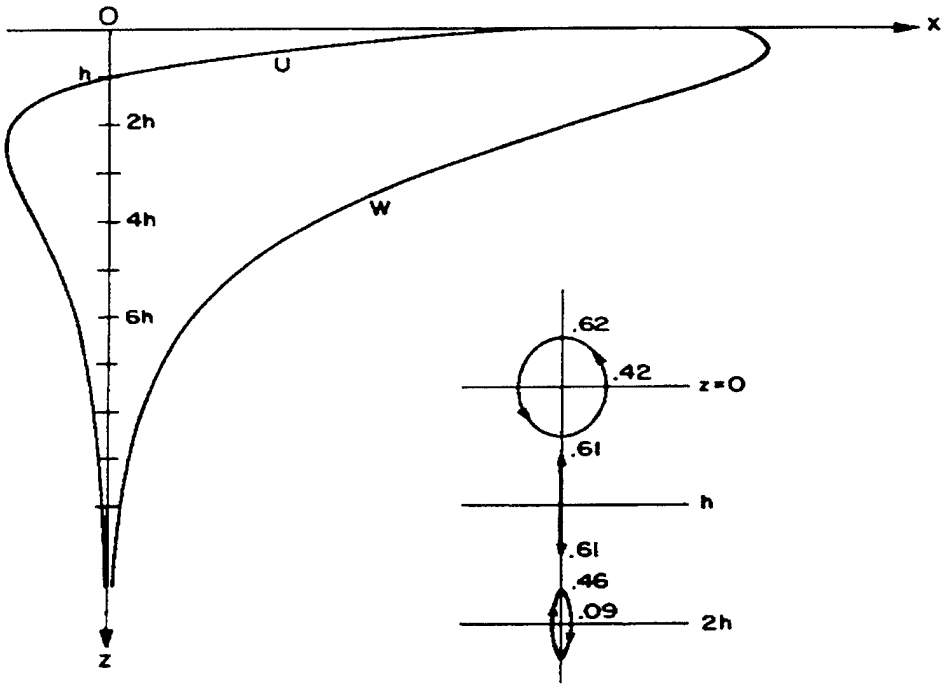

Figure 2.3. The horizontal (U) and vertical (W, down) displacements for Rayleigh waves in a homogeneous half-space. U vanishes at depth h. The path of the particles is elliptic retrograde for $z < h$ and elliptic direct (prograde) for $z > h$. From Ref. [19].

2. Love Waves

The Rayleigh waves described above are guided by a single boundary, the free surface. A ducted wave, however, is an interface wave that propagates in a duct, or wave guide, between two boundaries. Love waves, named after the British theoretical physicist A. E. H. Love who first gave the theory of their existence in 1911, are surface waves which are observed when there is a low shear wave velocity layer overlying a high shear wave velocity substratum. The wave guide is thus formed by the surface of the earth and the underlying velocity interface. The particle motion, like SH waves, is horizontal and perpendicular to the direction of propagation (see Figure 2.1), however, the displacement of Love waves decreases with depth. All love waves are dispersive, with the velocity increasing with wavelength. The Love wave speed ranges from V_s (shear wave velocity) in the upper layer for short wavelengths to V_s in the lower layer for long wavelengths. [Ref. 17]

C. SURFACE WAVE APPLICABILITY TO SEISMIC SONAR

The seismic waves described above are normally discussed in the context of earthquakes or major underground explosions. The concept of a seismic sonar requires a man-made source, or array of sources, to generate seismic waves, and receivers to record the energy scattered from targets, such as buried land mines. An illustrative example of a seismic energy source would be the wave field generated by a horizontal circular footing, such as a mechanical "shaker" that could provide an impulse at the surface of the earth. The seismic energy profile of such a footing has been extensively studied, and the basic features of this wave field at a relatively large distance ($> \sim 2.5\ \lambda$) are shown in Figure 2.4. It can be seen that the body waves propagate radially outward from the source along a hemispherical wave front and the Rayleigh waves propagate radially outward along a cylindrical wave front. While such sources clearly generate both body and surface waves, Rayleigh waves are the cornerstone of the seismic sonar because they carry a

majority of the energy, they are confined to the surface, and they have polarization features that make them easily to identifiable.

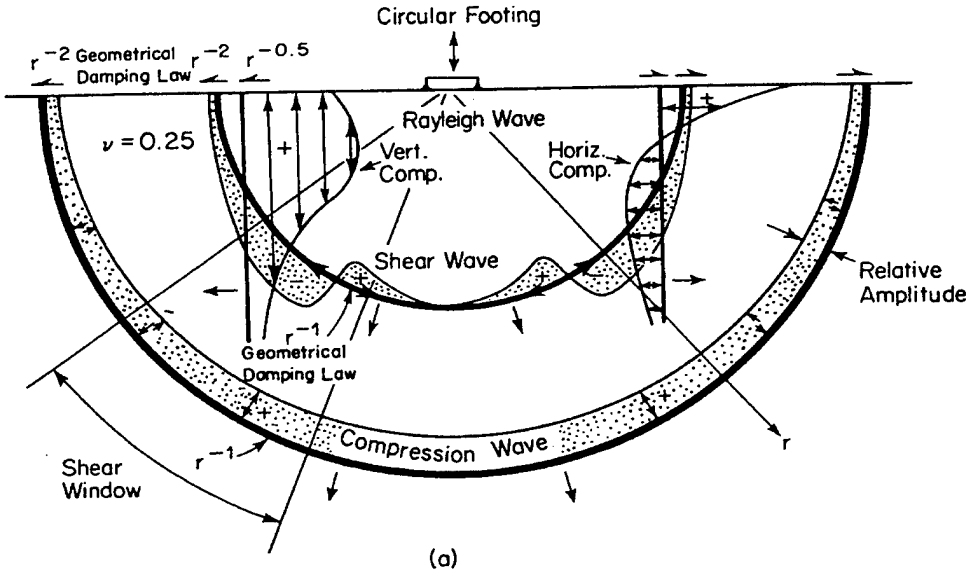

Wave Type	Per Cent of Total Energy
Rayleigh	67
Shear	26
Compression	7

Figure 2.4. Distribution of displacement waves from a circular footing vibrating on homogeneous, isotropic, elastic half-space. From Ref. [20].

1. Far Field Energy

In order to use seismic energy to detect buried mines, one must take advantage of how nature distributes the source energy. As mentioned above, the amplitude of the body waves decreases in proportion to 1/r, whereas the amplitude of the Rayleigh wave decreases in proportion to $1/\sqrt{r}$. Therefore, beyond about 2.5 wavelengths from the

source, Rayleigh waves carry about 67% of the seismic energy at the surface (see Figure 2.4). Note that with the horizontal orientation of the source footing, very little SH wave energy, and thus very little Love wave energy would be generated. However, given a vertical orientation of the source, one could place a majority of the energy at the surface into Love waves instead of Rayleigh waves.

2. Surface Confinement

A major advantage of using surface waves to detect buried objects is the fact that they decay exponentially with depth and thus do not reflect off of the complex topography of the substructure. Figure 2.5 illustrates how surface waves lend themselves to the task of locating buried ordnance in the shallow surf zone, in beach sediments, and on land. Because they travel along the interface, surface waves are not strongly affected by features deeper than about two wavelengths. Therefore, at selected wavelengths, one can attribute scattering of surface waves to come from objects buried near the surface, be they natural or manmade.

3. Vector Wavefield Features

As shown in Figure 2.3, a seismic source will generate both body and interface waves. The preceding discussion highlights the fact that most of the energy resides in the surface waves and these waves will be essentially unaffected by any complex structure at depths greater than a few wavelengths. However, the body waves will spread hemispherically, and through multiple reflections from substructure, may exist at the same time as the desired surface wave return from a buried object. In the case of Rayleigh waves however, the desired energy scattered from the buried object can be distinguished from extraneous body wave reflections through a process called vector polarization filtering. The signal processing advantages of this feature will be discussed in detail in a later section.

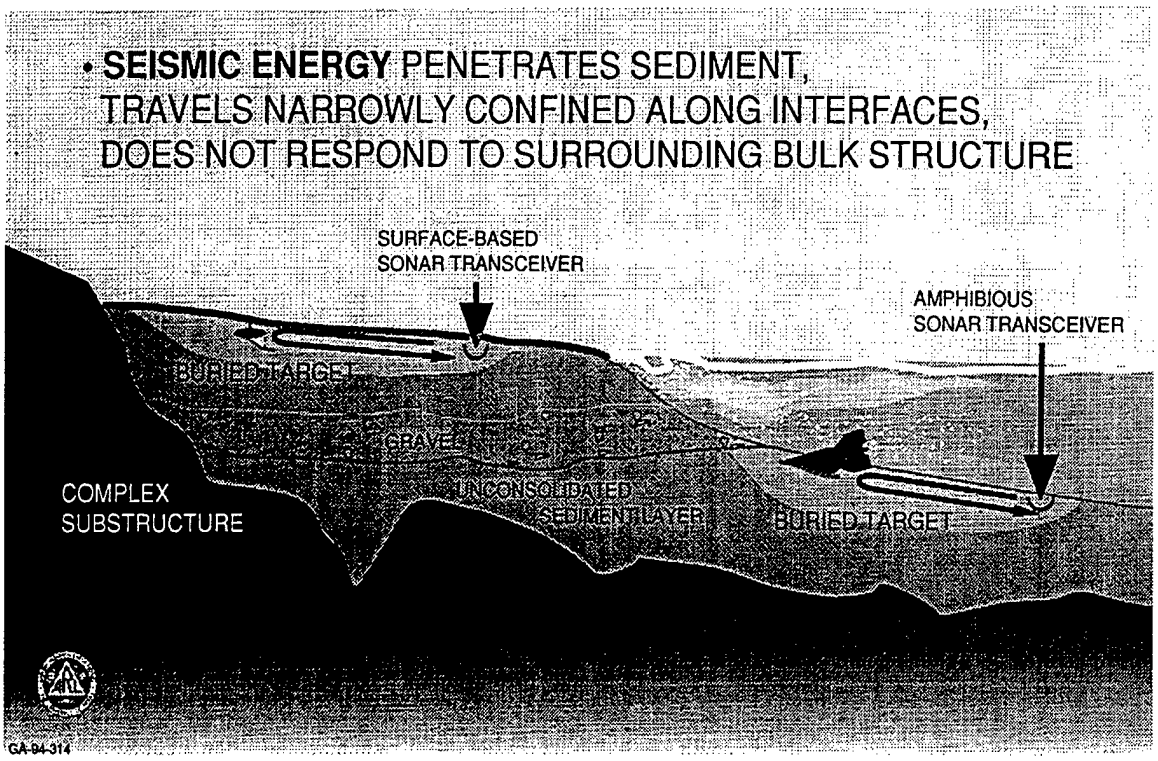

Figure 2.5. Concept for seismic interface wave sonar.

THIS PAGE INTENTIONALLY LEFT BLANK

III. PREVIOUS AND CONCURRENT RESEARCH

This thesis is a direct continuation of a research project that began at the Applied Research Laboratories of the University of Texas at Austin (ARL:UT) where the theory and signal processing techniques for the seismic sonar system were introduced in 1996. Since then, three graduate students at the Naval Postgraduate School (NPS) have continued to experiment with the source and receiver configurations in order to advance the concept of using seismic interface waves (surface waves) to locate and measure the target strength of buried objects. The following sections briefly discuss these contributions to the ongoing effort to detect buried mines in the surf zone, on the beach, and on land.

A. ARL:UT

Proof of concept studies for the seismic sonar were conducted by ARL:UT in the early 1990s to investigate the possibility of using Rayleigh waves to detect buried mines and ordnance. [Ref. 11] Their experimental apparatus is shown in Figure 3.1. The seismic source consisted of a six-inch by eight-inch "exciter foot" with numerous protruding nails, driven by an electro-mechanical transducer. The receiving array consisted of three, three-axis seismometers. The buried target was a mine-sized titanium cylinder that was buried with the top flush with the sand surface.

ARL:UT discovered that the received signals contained complicated wavefields with reverberation and body wave reflections that tended to mask the target echo. In order to isolate the target signal, they used various signal processing techniques including coherent subtraction and vector polarization filtering. [Ref. 11] In doing so, they were able to successfully detect the buried mine-like object. These same methods are applied in this thesis and will be discussed in a later section.

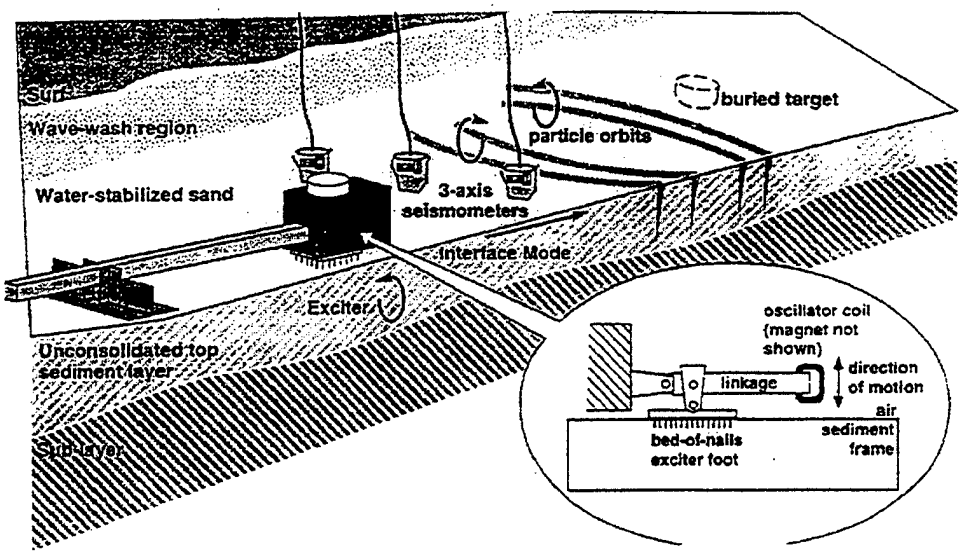

Figure 3.1. ARL:UT seismic sonar experiment configuration From Ref. [11].

B. NAVAL POSTGRADUATE SCHOOL (NPS)

After the promising results described above concerning the use of Rayleigh waves to detect buried objects, one of the key researchers at ARL:UT, Dr. Thomas G. Muir came to NPS in 1997. As Chair Professor of Mine Warfare and principal investigator (PI) for buried mine detection, he has led numerous graduate students in research to further develop the theory and practical applications of the seismic sonar. Professor Muir teamed up with Professor Steven Baker, who, as Co-PI, has made significant contributions in transduction and computer electronics for data acquisition. Professor Baker has also co-supervised graduate students working on the seismic sonar development. Also contributing to the seismic sonar research were Professor Clyde Scandrette from the Mathematics Department, and Professor Monique Fargues, and her students, from the Electrical Engineering Department. They have contributed in the areas of target strength modeling and signal processing respectively.

1. Discrete-Mode Source Development

In 1998, Lt. Frederick E. Gaghan (USN) focused on developing a seismic source that preferentially excites interface waves. [Ref. 12] His work was geared toward the design, fabrication, and testing of numerous source configurations with the intent of selectively generating Rayleigh waves. His final source configuration, shown in Figure 3.2, consisted of two commercially available, moving magnet, inertial reaction force transducers (bass shakers), mounted on an aluminum base at 45 degree angles.

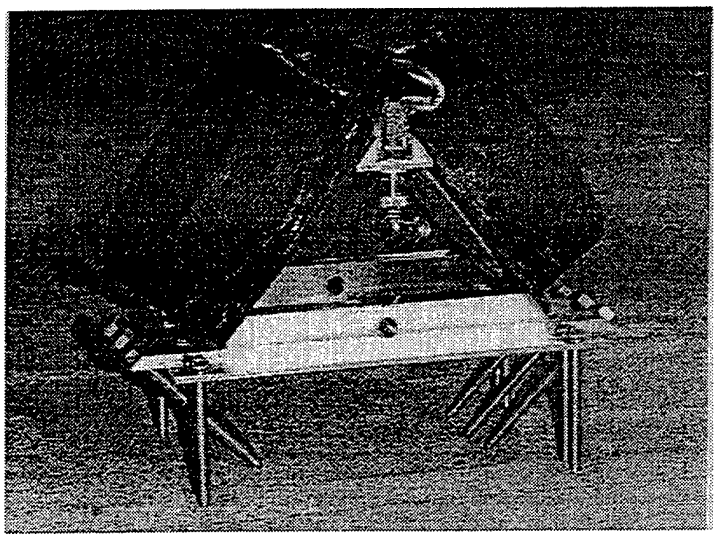

Figure 3.2. Discrete-mode seismic sonar source design From Ref. [12].

However, even after driving the discrete-mode source under several different modes of excitation, in an attempt to mimic Rayleigh wave motion, Lt. Gaghan found that the sources still generated all types of seismic waves. Interestingly, he found that the medium itself acted as a filter in such a way that, beyond a few wavelengths, surface waves overshadowed body wave arrivals at the surface. This concept illustrates how the earth itself propagates a majority of earthquake energy along the surface in the form of

Rayleigh waves, more commonly known in oil exploration as "ground roll". Lt. Gaghan concluded that a discrete-mode force might be effective if there was an automatic feedback control mechanism to suppress the unwanted modes. He also stated the need for higher quality, greater force producing, sources with better sediment coupling.

2. Source Developments and Target Strength Measurements

In December 1998, two graduate students Lt. S. Michael Fitzpatrick (USN), and MAJ Patrick W. Hall (USMC), concurrently published results from continued experimentation with the seismic sonar.

Lt. Fitzpatrick [Ref. 13] developed two seismic sources that utilized commercially available linear magnetic actuators, capable of delivering 25 pounds of force. The actuators were modified significantly, resulting in the simple, sturdy, direct-drive, linear system shown in Figure 3.3. The actuator was mounted on roller bearing within a plastic tube, and coupled to a protruding actuator rod through a waterproof rubber diaphragm. The square plate attached to the end of the actuating rod was then buried about 3-4 inches beneath the surface of the sand and driven with a sinusoidal force input to generate seismic waves. This unit was tested and used in several seismic wave generation and propagation experiments in the surf zone of the Navy Beach in Monterey, CA.

MAJ Hall furthered the research by employing a seismic sonar system on the Navy Beach to measure the target strength of a compressed gas cylinder and a gunpowder keg. [Ref. 14] He used the linear force actuators designed by Lt. Fitzpatrick as sources in conjunction with a three-axis seismometer and recorded reflected seismic wave energy from the buried targets. The hollow targets were designed such that lead blocks could be placed inside without excavating the entire target. Using vector polarization filtering to separate the reflected Rayleigh waves from the body waves, MAJ Hall was able to measure target strength as a function of mass inside the targets. The target strength was generally observed to increase with increasing target mass as shown in Figure 3.4, although the powder keg target strengths flattened out at high mass loadings, for reasons that have not yet been explained.

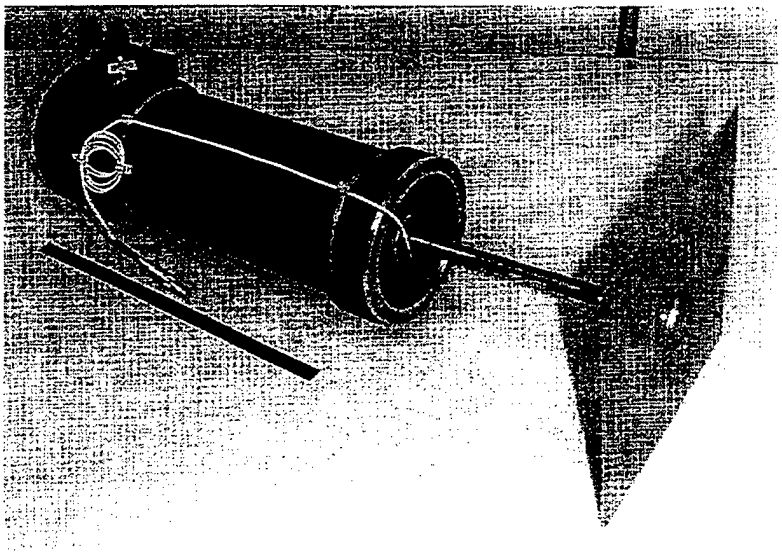

Figure 3.3. The fully assembled watertight seismic sonar source. From Ref. [13].

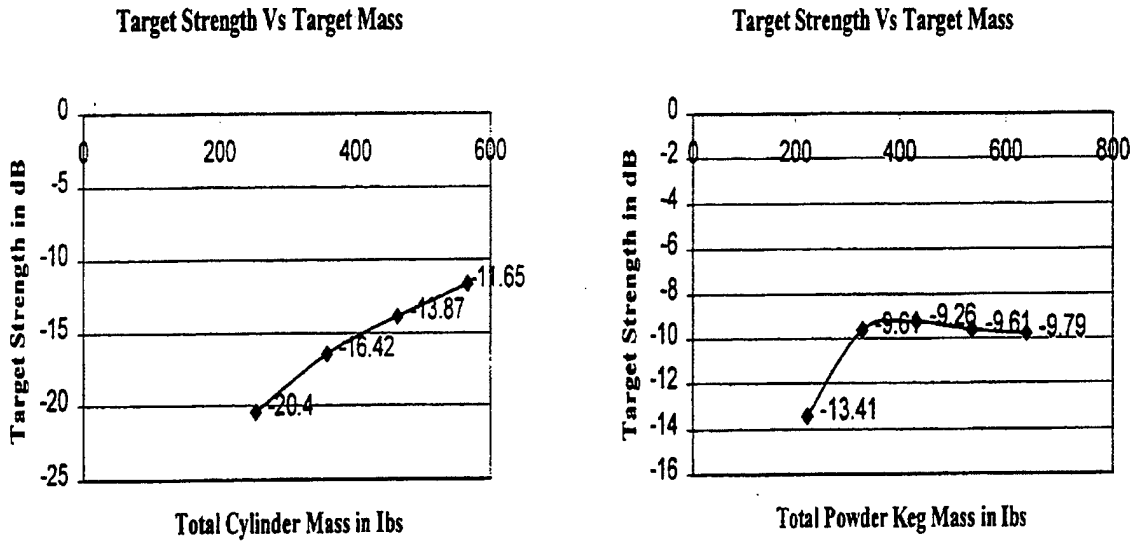

Figure 3.4. Target strength vs. target mass: gas cylinder and powder keg. From Ref. [14].

3. Target Classification

An important aspect of using seismic sonar to detect buried mines is the ability to discriminate between man made and natural buried objects. Professor Monique Fargues and her students are working on digital classification schemes to address this problem. In October, 1999, Professor Fargues and her student, Lt. Michael Zambartas, Hellenic Navy, published preliminary classification results in Lt. Zambartas' thesis [Ref. 21] and a joint paper [Ref. 22] presented at the 33rd Asilomar Conference on Signals, Systems, and Computers in Pacific Grove, California. Their work investigated the application of Hidden Markov Models (HMM) to target classification problems.

Hidden Markov Model theory has been used extensively in the last decade to model the temporal structure and variability of speech and other signals. Using the data collected by MAJ Hall during his target strength experiments, Lt. Zambartas and Professor Fargues developed their own HMM codes using MATLAB to differentiate between the two types of mine-like objects (gas cylinder and powder keg). Their results indicated an ability to recognize the object type, independent of the mass load, with 97% accuracy. They also used a back-propagation neural network implementation and found similar results, although at slower processing speeds.

One of professor Fargues' current students, Lt. Craig Wilgenbusch (USN), is continuing the effort to classify targets. He is investigating statistical classification methods and reflection harmonic analysis in attempt to develop an automated detection scheme that would discriminate between man-made and natural objects.

4. Data Acquisition

The seismic sonar concept for this research includes both source and receiving arrays. Currently, a separate function generator drives the source array and the received signals are recorded with an eight-channel data acquisition system (see Chapter IV for a complete description of the current equipment configuration). Professor Steve Baker, of the NPS Physics Department, is currently assembling a modular, expandable acquisition

and control system that will greatly expand the capabilities of the seismic sonar research tool. The system will initially have 16 output and 32 input channels synchronized to a common clock. Once completed, this acquisition and control system will be programmable using MATLAB's new Data Acquisition Toolbox, and will enable the user to simultaneously control both the source waveforms and the recording parameters. Such advances will introduce vital capabilities such as arbitrary waveform generation and electronic beam steering.

5. Finite Difference Modeling

Professor Clyde Scandrette, NPS Department of Mathematics, is working on a three dimensional finite difference code for solving the time-dependent scattering from a buried homogeneity in an isotropic medium. Professor Scandrette is the Chairman of the NPS Undersea Warfare Academic Group and has begun developing this code to model the propagation and reflection properties of both body and surface waves in a sand medium like the Navy Beach Research Facility. This model will provide a powerful theoretical tool to compliment the experimental data from this and previous research.

6. Mine Burial

The ability to predict the rate of mine burial would provide MCM forces with important information concerning the optimal timeframe to search for recently deployed mines. In September 2000, LCdr Wayne L. Plager (USN) published results of experiments conducted jointly under Professor Muir of the NPS Physics Department, and Professor Thorton of the NPS Oceanography Department [Ref. 23]. He measured the volumetric rate of scour and burial of the Mk-63 mine shape in the swash and surf zone in two separate experiments on the Navy Beach Research Facility. After placing the mine shape on top of the sand in the surf zone, LCdr Plager recorded orbital velocities of

the waves with an Acoustic Doppler Velocimeter and manually measured the three dimensional scour with continuously recorded, high-resolution video. He was able to determine that the Mk-63 mine shape was completely buried in 24 hours to a depth of about 4 in (10 cm).

IV. FIELD ENVIRONMENT AND EQUIPMENT REQUIREMENTS

A. TEST FACILITY

Many of the equipment testing experiments and preliminary source development tests were conducted in a large sand tank located in the NPS acoustics lab. The tank, shown in Figure 4.1, is very useful for such tests, but is inadequate for conducting actual target location experiments with the seismic sonar. The tank is undersized with respect to seismic wavelengths and the walls and floor represent a source of multiple signal reflections that mask target returns.

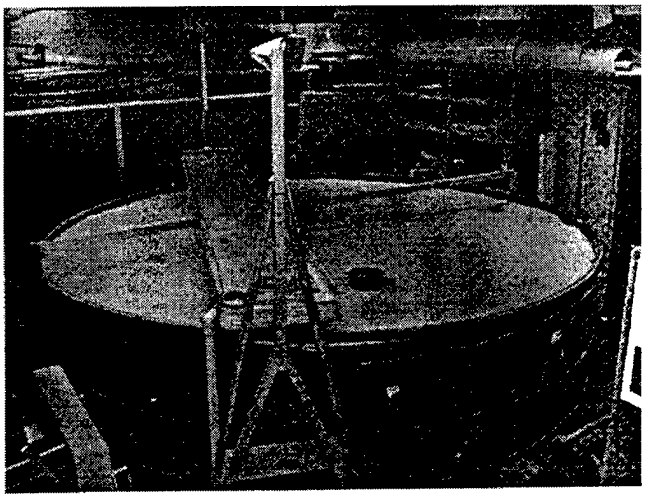

Figure 4.1. Laboratory sand tank.

B. FIELD EXPERIMENT SITE

To avoid the unnatural consequences of working in the sand tank, seismic sonar experiments were moved to field. The field site for this research was the U.S. Navy research facility at Del Monte Beach, which is located adjacent to the Naval Postgraduate

School. Del Monte beach is located on the south shore of the Monterey Bay facing north. (see Figure 4.2) Waves incident on the beach experience strong refraction as they pass over the Monterey Bay submarine canyon, and are protected by Point Pinos headland. This results in waves approaching the beach at near normal wave incidence with weak longshore currents. The mean beach slope is 1:40 and the mean grain size is 0.2 mm. The beach is subjected to diurnal and semidiurnal tides with mean tides of 2 meters. [Ref 23] In order to conduct research in this realistic setting, it was necessary to quantify some important characteristics of the beach environment, such as Rayleigh wave velocity and background noise spectrum.

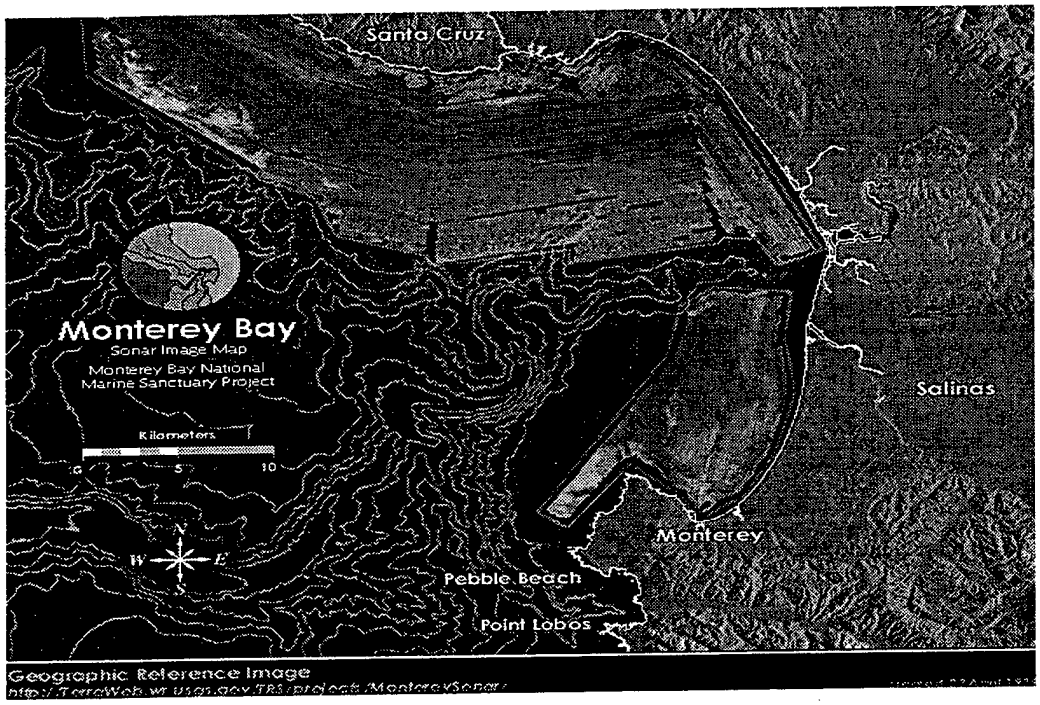

Figure 4.2. US Geographic Survey chart of Southern Monterey Bay with sonar Bathymetry. From Ref [24].

1. Rayleigh Wave Velocities

Based on previous research, the driving frequency used for these experiments was in the low audio band, centered at 100 Hz. This is not to say that 100 Hz is the ideal frequency and a frequency sensitivity test is a desired topic for future research. Lt. Fitzpatrick [Ref. 7] conducted extensive field tests to record the Rayleigh wave arrival times as a function of source-geophone separation. From this data, he estimated the propagating velocity of the Rayleigh wave mode at 100 Hz to be 80 m/s. However, further velocity experiments concluded that the velocity of the beach sediments is quite dynamic and can change within a tide cycle. As the tide rises and falls, so does the water table and the moisture content of the sediments, especially the rise and fall of the totally saturated substrate level. As a result, wave speed can change even within the span of an experiment. The value of 80 m/s is a good average Rayleigh wave speed for the navy beach site, however, the uncertainty applied to this value is at least $\pm$ 10 m/s.

2. Background Noise

In choosing field equipment such as seismometers and portable power sources, it is important to know the frequency of the background noise caused by natural (waves, wind, etc) and man made elements. The spectral analysis of noise samples recorded at the field site with a velocity sensitive seismometer is shown in Figure 4.3. The plot shows the incoherent average of the horizontal and vertical components. A majority of the noise lies between 5 – 20 Hz, which is well below the source frequency (100 Hz) that was used for this research. In order to reduce this background noise, all of the signals from the seismometer array were filtered, passing frequencies between 30 and 300 Hz, prior to recording with the data acquisition system.

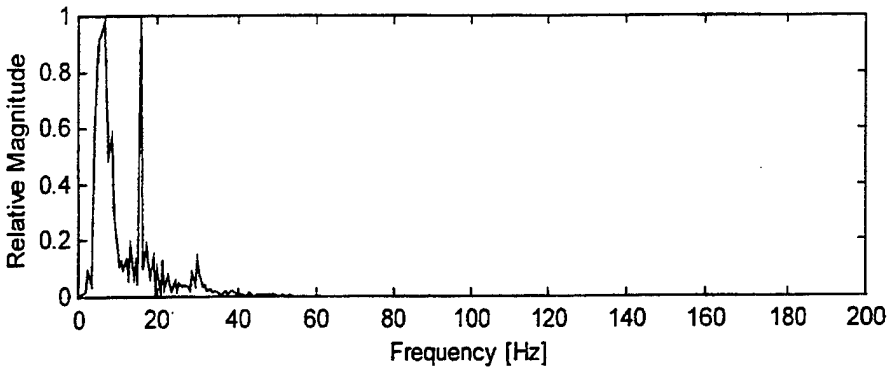

Figure 4.3. Background noise of beach research site. From Ref. [6].

C. FIELD RESEARCH TOOL

The challenge of designing and building a seismic sonar research tool that was both self contained and deployable was quite formidable. The system, which had to be able to access the beach on an unimproved road and move across loose beach sands, had to have all of the necessary electrical power and electronic equipment on board. Over the past two years, the configuration has gone through many evolutionary stages, the current of which is shown in Figure 4.4. The prime mover of the system is a John Deere, 4x6 "Trail Gator", in the bed of the which is depicted a Honda 2500 Watt A/C power generator that is remotely deployed during experimentation. The white trailer houses all of the necessary computer and electronics equipment for seismic sonar research tool. Figure 4.5 shows the contents of the trailer which was designed to the largest possible dimensions that would fit through the double doors entering both the NPS physics, oceanography and electrical engineering building (Spanagel Hall) and the acoustics laboratory (sand tank room) in its basement. This concept enabled the entire equipment suite to be kept in the laboratory for testing or demonstrations, and wheeled out to the loading dock to be lowered with the dock crane for movement to the field site.

Figure 4.4. The author and co-researcher with the seismic sonar research tool.

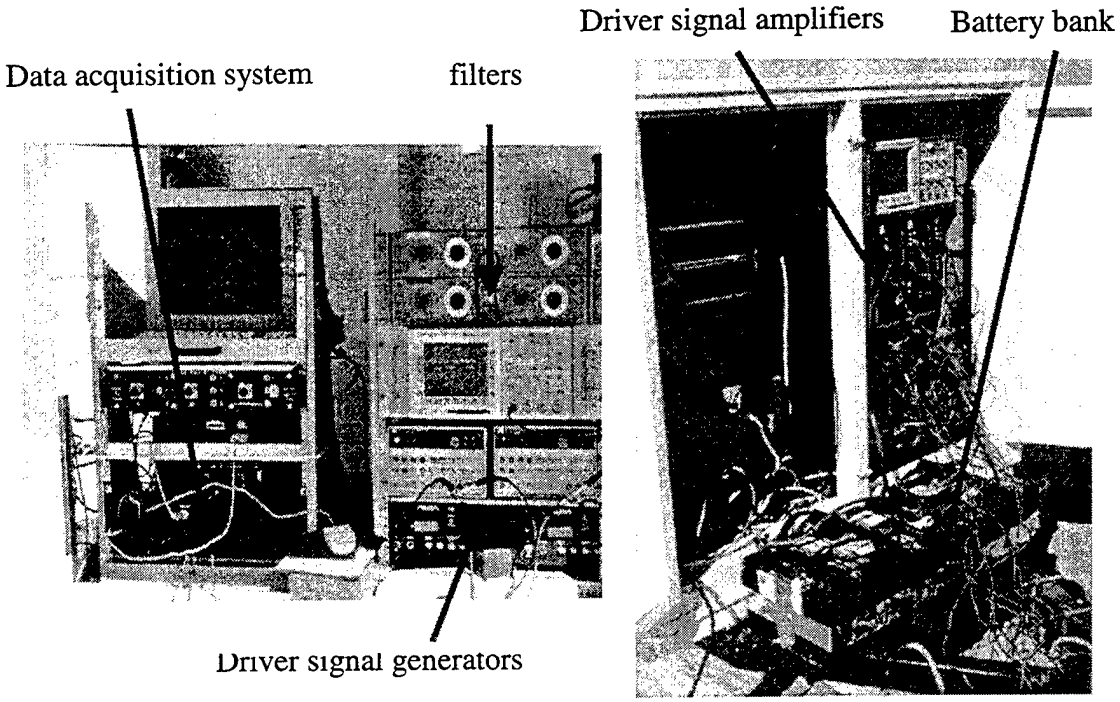

Figure 4.5. Contents of research tool equipment trailer.

The data acquisition system is Signal Processing System's SPS390, a 16-bit, 0-40 kHz analyzer capable of recording eight channels of data. The Honda gasoline generator powered this system, and all of the supporting electronics, with the exception of the signal amplifier bank. The amplifier bank, consisting of eight commercially available Alpine 500 watt power amplifiers, required significant amounts of peak current during pulse transmission (about 20 amps each) to drive the source array elements (the sources are discussed in a later section). To support the current requirements, a bank of four automobile batteries was fixed to the trailer. A photo of the seismic sonar research tool in the fully deployed configuration on the Navy beach experiment site is shown in Figure 4.6.

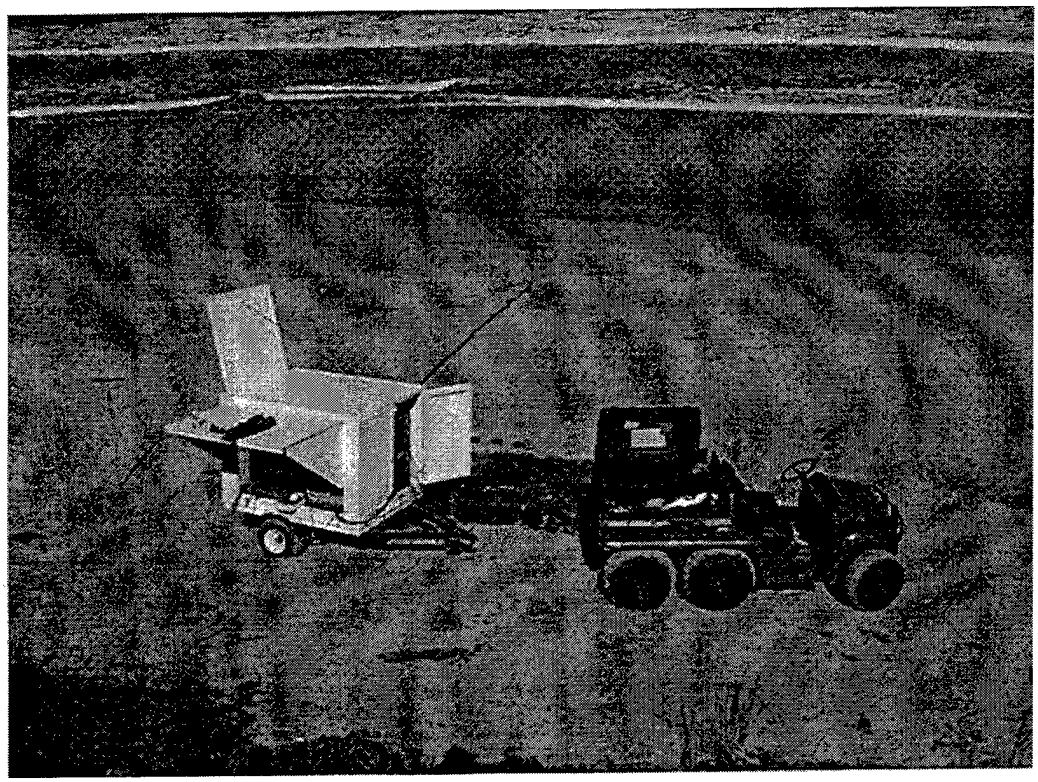

Figure 4.6. Fully deployed seismic sonar research tool.

D. GEOPHONE TESTING

The three-component seismometers used in this research contain two horizontal (x and y) and one vertical (z) geophone potted inside a watertight cylinder.

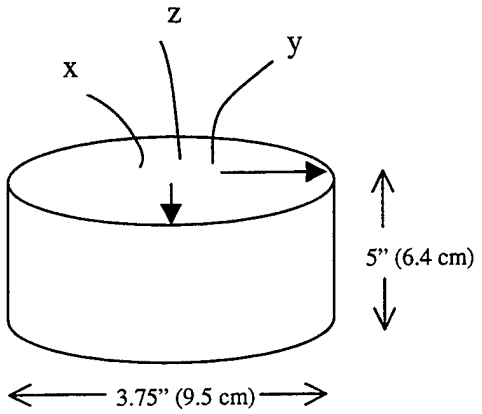

Figure 4.7. Three component seismometer.

The individual geophones inside the seismometer are SENSOR Nederland products, specifically the SM-6, 4.5 Hz model, marketed in the U.S. by INPUT/OUTPUT, INC. The specifications for this model (found in Appendix A) show that the maximum tilt angle for the specified functionality is 0 degrees, and the typical spurious frequency (where geophone coupling problems arise) is 140 Hz. Because the realistic beach environment has uneven terrain with unpredictable localized slopes, and the spurious frequency is fairly close to the experimental operating frequency of 100 Hz, laboratory tests were conducted to determine the sensitivity of the geophones to tilt angle.

Individual geophones (that were not yet potted into a seismometer), were fixed to an Acoustics Power Systems, INC., Perma-Dyne Model 120S shaker table via a Bruel & Kjaer Type 8305S calibration accelerometer that had no sensitivity to tilt angle. The accelerometer was amplified with a Kistler Type 5010 Dual Mode Amplifier. The table was driven by a frequency swept sinusoidal signal and the output from the geophone was compared with the output from the integrated accelerometer. Since the geophone measures velocity and the accelerometer acceleration, the accelerometer output signal

was integrated using a low-pass filter in order to make this comparison possible. Finally, the phase between the geophone output and the accelerometer output, as well as their amplitude ratio, were plotted as a function of frequency.

Figure 4.8 shows the reference plot of zero degree tilt angle for the horizontal SM-6 geophone for a frequency range of 50–250 Hz. This plot would serve as the basis from which to measure any variations of the geophone output as a function of tilt angle. As shown in Figure 4.9, only a 2 degree tilt angle caused an irregularity in both the phase and gain. Note that the spurious frequency appears to fall between 170 and 190 Hz, which, while slightly higher than the manufacturer's specifications, is still close enough to 100 Hz to be carefully avoided. Two actions resulted from this experiment. First was the addition to the field operating procedures that the seismometers would be carefully deployed with a leveling device to ensure that the tilt angle was minimized. Secondly, different geophone models (same manufacturer), with little or no tilt angle restrictions, were ordered and tested in the same fashion as above.

The SM-11, 30 Hz geophone advertised 180 degree tilt angle tolerance with a spurious frequency of > 500 Hz. Again, the phase relationship and amplitude ratio between the geophone and the accelerometer were observed as a function of angle. Beginning with zero degrees, tilt angles were increased to 90 degrees by 10-degree increments and there was no variation in the phase relationship. A very slight variation in the amplitude ratio (gain) was noted when the tilt angle was 90 degrees. Figures 4.10 and 4.11 show plots of the amplitude ratio between the horizontal SM-11 and the calibration accelerometer, as a function of frequency, for zero degree and 90 degree tilt respectively. The spike in Figure 4.11 is quite small and the frequency is well above the current experimental operating frequency of 100 Hz. The same test was conducted for the vertical model of the SM-11 and the results were identical to those for the horizontal model. It can be concluded then, that the vertical and horizontal models of the SM-11 can be oriented at any angle and still adhere to the advertised specifications. As a result, 51 SM-11, vertical model geophones were ordered and upon assembly into seismometer configurations, will be available for future experiments (specifications for SM-11 in Appendix A).

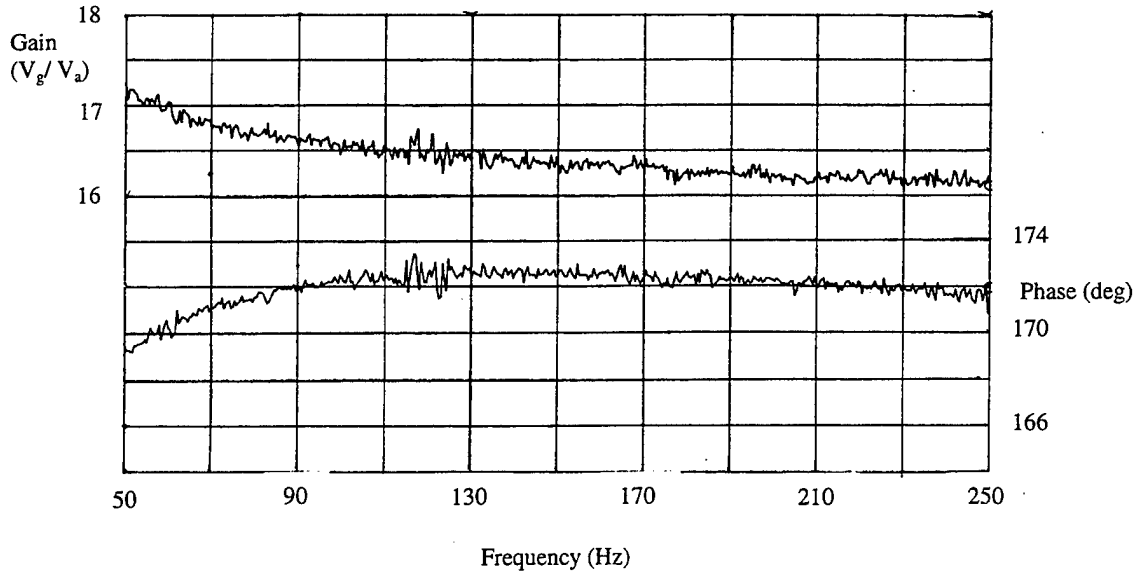

Figure 4.8. Phase relation and amplitude ratio between horizontal SM-6 geophone at zero degree tilt and a Bruel & Kjaer Type 8305S calibration accelerometer.

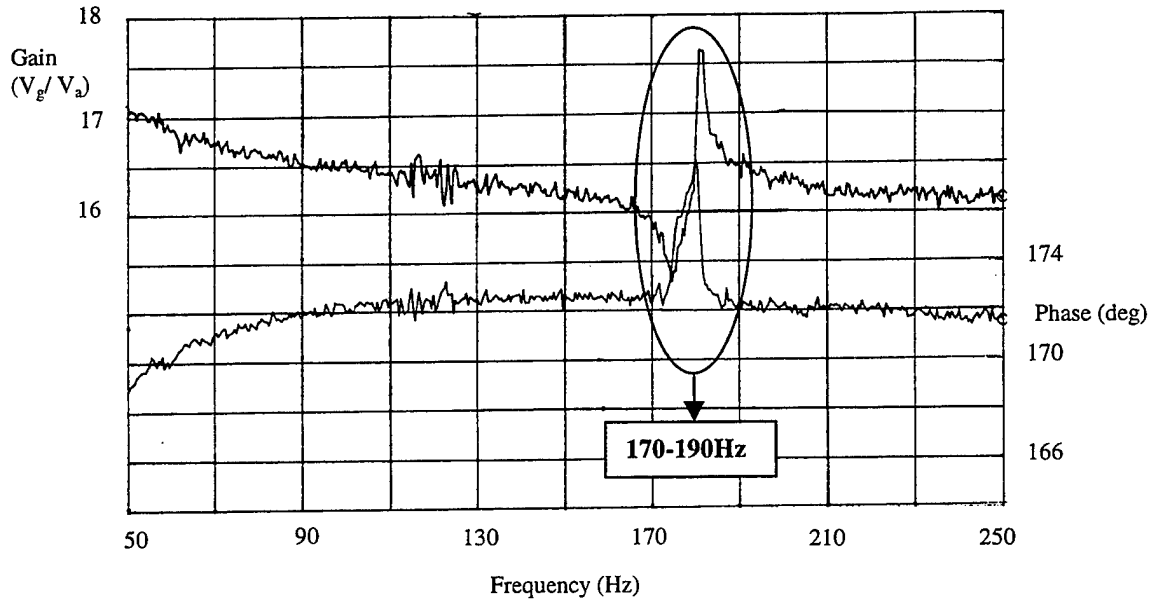

Figure 4.9. Phase relation and amplitude ratio between horizontal SM-6 geophone at two degree tilt and a Bruel & Kjaer Type 8305S calibration accelerometer.

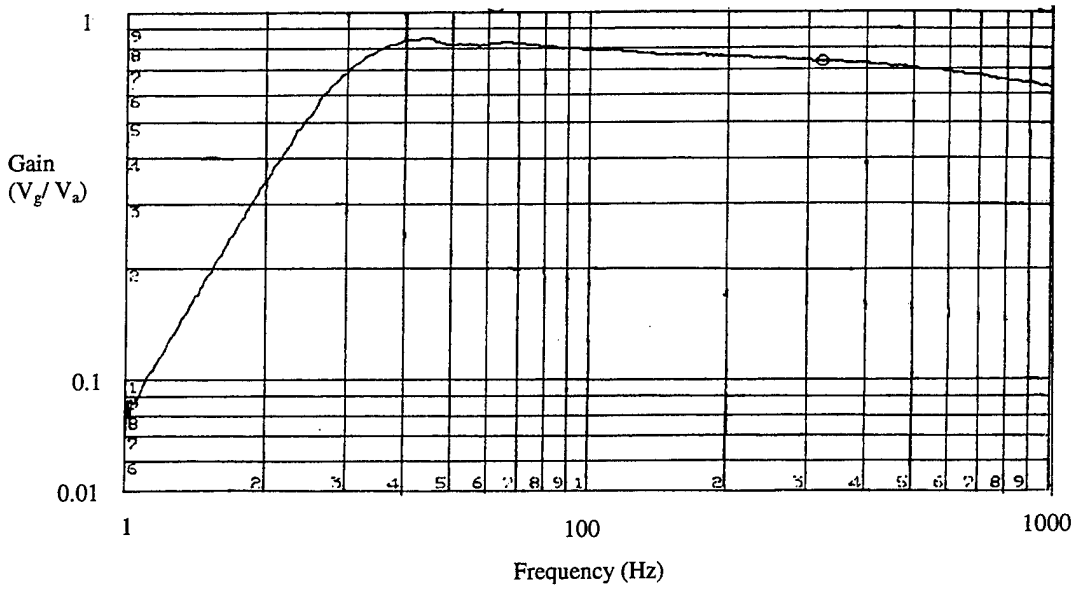

Figure 4.10. Amplitude ratio between horizontal SM-11 geophone, at zero degree tilt, and a Bruel & Kjaer Type 8305S calibration accelerometer.

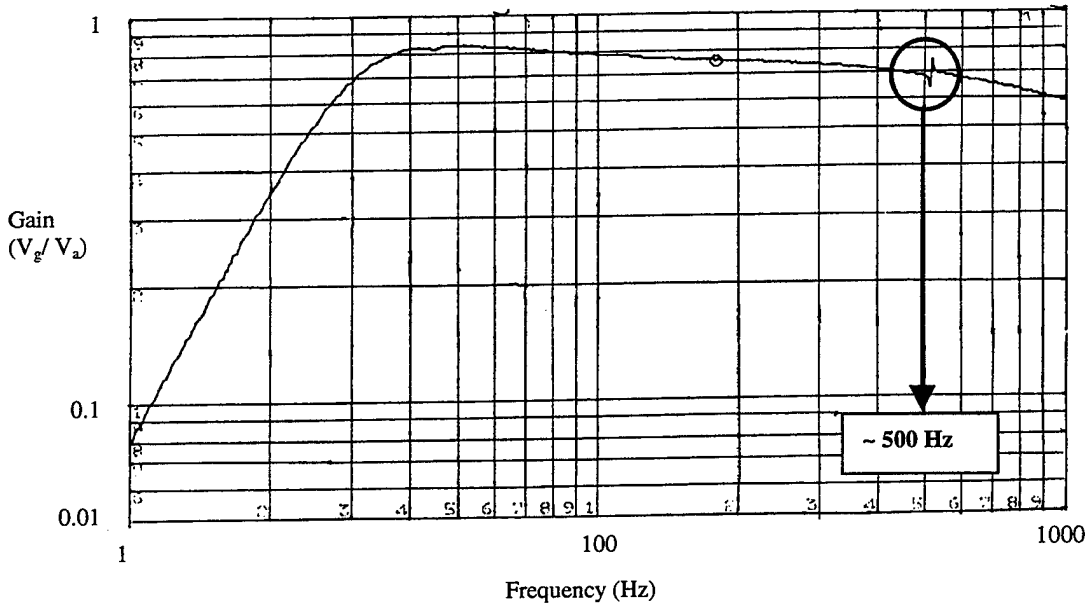

Figure 4.11. Amplitude ratio between horizontal SM-11 geophone, at 90 degree tilt, and a Bruel & Kjaer Type 8305S calibration accelerometer.

E. SOURCE DEVELOPMENT

The design and implementation of the seismic sources has been the focus of much of the seismic sonar research. As discussed in Chapter III, two of the three previous graduate students at NPS have dedicated time and resources toward finding the most effective way to generate Rayleigh waves with good elliptical particle motion. For this research, as in the work by Lt. Gaghan [Ref. 12], the Aura Systems Inc. Bass Shakers were used as sources. The Bass Shaker is a moving magnet transducer that is used as a low frequency vibration source for the car audio industry. Figure 4.12 shows a cutaway view of the mechanical components of the shaker.

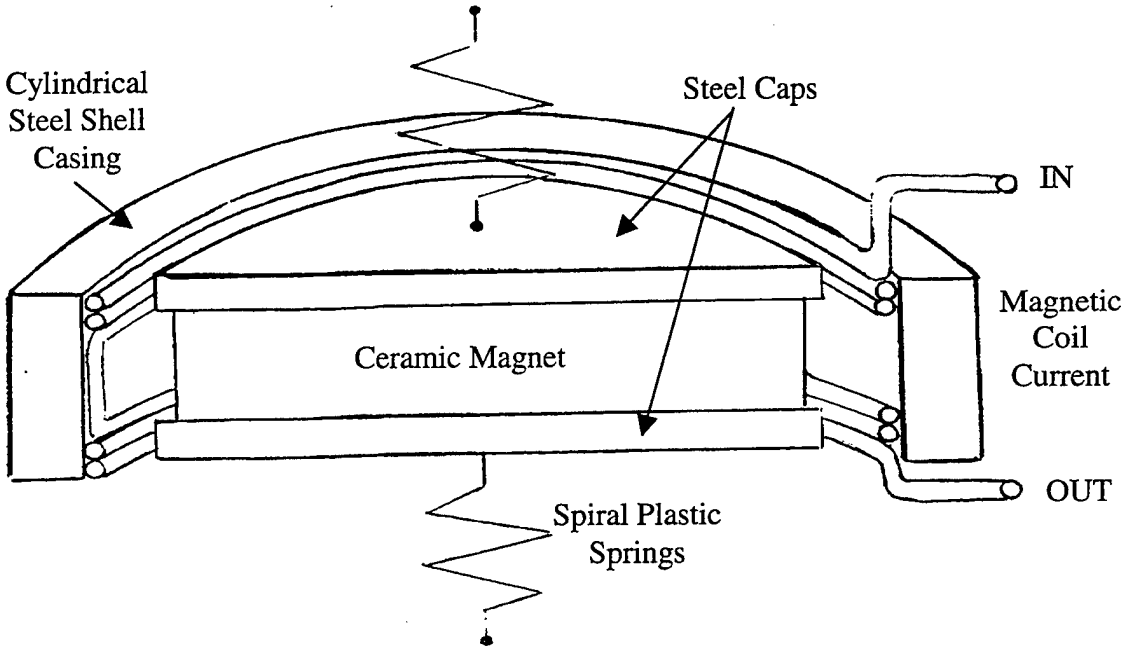

Figure 4.12. Perspective section of mechanical components of Bass Shaker.

A cylindrical ceramic magnet, sandwiched between two steel caps, is surrounded by a cylindrical steel shell that is lined with current carrying wires. The wires are oriented such that the direction of the current flow near the top of the magnet is opposite to the flow near the bottom. The top and bottom of the magnet "sandwich" are coupled to the outer shaker housing with spiral plastic springs. The forces generated by this configuration are graphically illustrated in Figure 4.13.

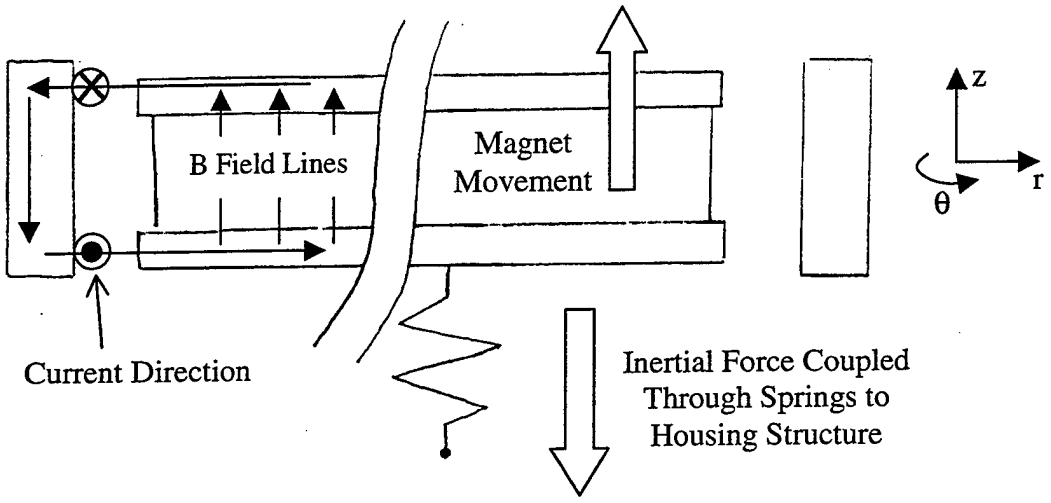

Figure 4.13. Cross section of magnetic field and forces.

The steel caps and casing shape the magnetic field to be radial outward (top of magnet) and inward (bottom of magnet). The current through the reverse-wired coil, thus provides a resulting magnetic force according to,

$$\vec{F}_{mag} = \vec{I}L \times \vec{B} \tag{4.1}$$
$$F_z = I_r L B_\theta - I_\theta L B_r = -I_\theta L B_r,$$

where $I_{r,\theta}$ and $B_{r,\theta}$ are the radial and azimuthal components of the current and magnetic field. Note that there is no radial current or azumuthal magnetic field so the first term in the expression for the force is zero.

The shaker generates a force output of about 10 lbs, independent of its mounting orientation. The manufacturer specifications for the Aura Bass Shaker are presented in Appendix B.

Since Lt. Gaghan found that it was difficult to preferentially excite Rayleigh waves and that the medium itself converted a simple vertical excitation into Rayleigh waves, with propagation to ranges needed for seismic sonar [Ref. 12], only vertical excitation was used in this research. This study focuses on creating an array of sources to maximize the signal on a specific axis, in a narrow, high resolution beam. The first attempt to use the shakers in an array entailed placing long screws through the shaker mounting holes so that they would remain stationary while vibrating on the surface of the sand. If this in not done, the shakers will "hop" up and down when they exceed 1g of gravitational attraction. They then lose contact with the sediments and literally "walk around" on the surface, leaving their intended position in the array. Figure 4.14 shows a single shaker configured for use in this way.

Figure 4.14. Bass Shaker with coupling screws.

When the shakers were used in this way, however, the resulting Rayleigh waves were unsatisfactory. The coupling mechanism was insufficient to dampen out the ringing of the shaker after the driver signal pulse. An illustrative means to observe the quality of Rayleigh waves generated by the sources is to generate a Hankel plot of the signal

measured by the seismometer at a distance at which Rayleigh waves should represent the predominant energy. A Hankel plot graphically displays the vertical and radial particle motion as a function of time. As mentioned in Chapter II, Rayleigh waves are vector fields, and have elliptical orbits. Figure 4.15 shows the vertical and radial particle velocity as a function of time recorded at a distance of 10 feet from an array of seven shakers placed on the surface of the sand. The subplot on the top right, known as a hodogram, shows the two-dimensional motion as if looking down the time axis. Perfect Rayleigh waves would appear as spirals in a Hankel plot (and an ellipse in a hodogram), and one can see that the motion from this source is rather random and not elliptical .

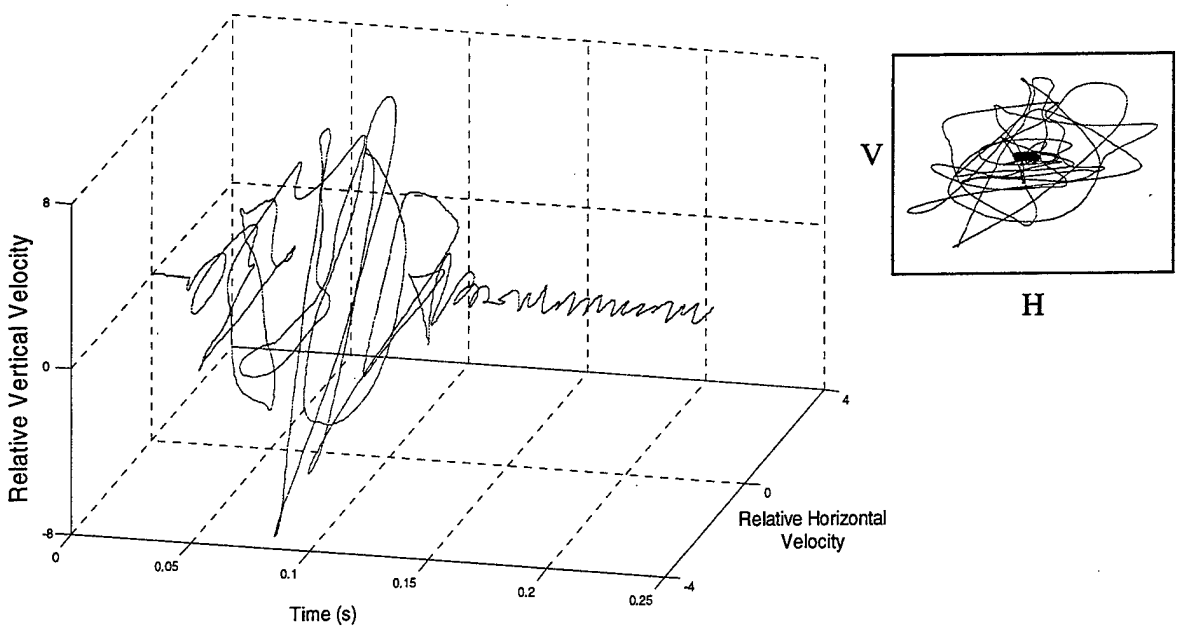

Figure 4.15. Hankel plot of seismometer velocity signals measured 10 feet (3 m) from array of Bass Shakers placed on top of the sand. Top right plot is the 2-D hodogram (V: vertical, H: horizontal).

Numerous attempts were made to modify or configure the bass shakers in order to improve the source-medium coupling, minimize the ringing, and obtain good Rayleigh wave particle motion. The present design is shown in Figure 4.16. Two bass shakers

were mounted on either side of a 12 inch (30.5 cm) diameter plywood disk, 1/4 inch (.63 cm) in thickness. One of the shakers was wired out of phase with the other such that, when driven with a sinusoidal signal, they vibrated in a "push-pull" configuration.

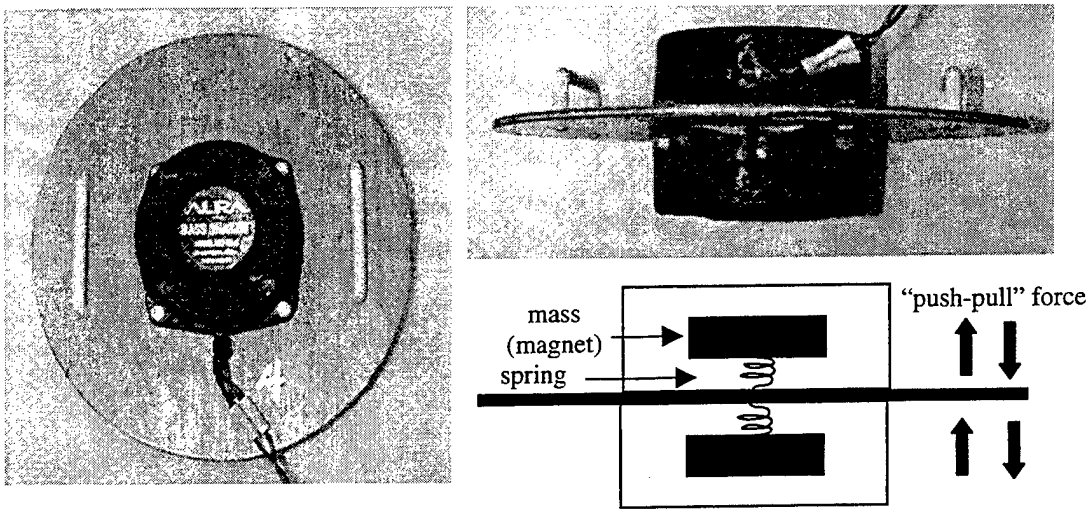

Figure 4.16. Current "bass shaker paddle" seismic source design.

Upon conducting tests of the "bass shaker paddle" in the sand tank with an attached accelerometer, it was discovered that if the sources were buried so that the top of the uppermost shaker was about two inches beneath the surface of the sand, the ringing was nearly all damped out and the coupling was much improved. Follow-on tests at the beach field site confirmed these results. Figure 4.17 shows an array of seven of the new sources arranged at half wavelength spacing. For a 100 Hz Rayleigh wave at a velocity of 70 m/s, one-half wavelength is about 14 inches (35.6 cm). For Rayleigh wave experiments, the sources were buried using a cylindrical coffer dam so that the paddle is parallel with the beach surface and the top shaker is two inches (5 cm) below the surface. In contrast to Figure 4.15, Figure 4.18 shows the much improved particle motion at a distance of 10 feet (on axis) from the array. Again, the vertical and radial particle motion is plotted as a function of time and the motion is clearly elliptical and retrograde.

Figure 4.17. Source employment with coffer dam (left) and array prior to burial (right).

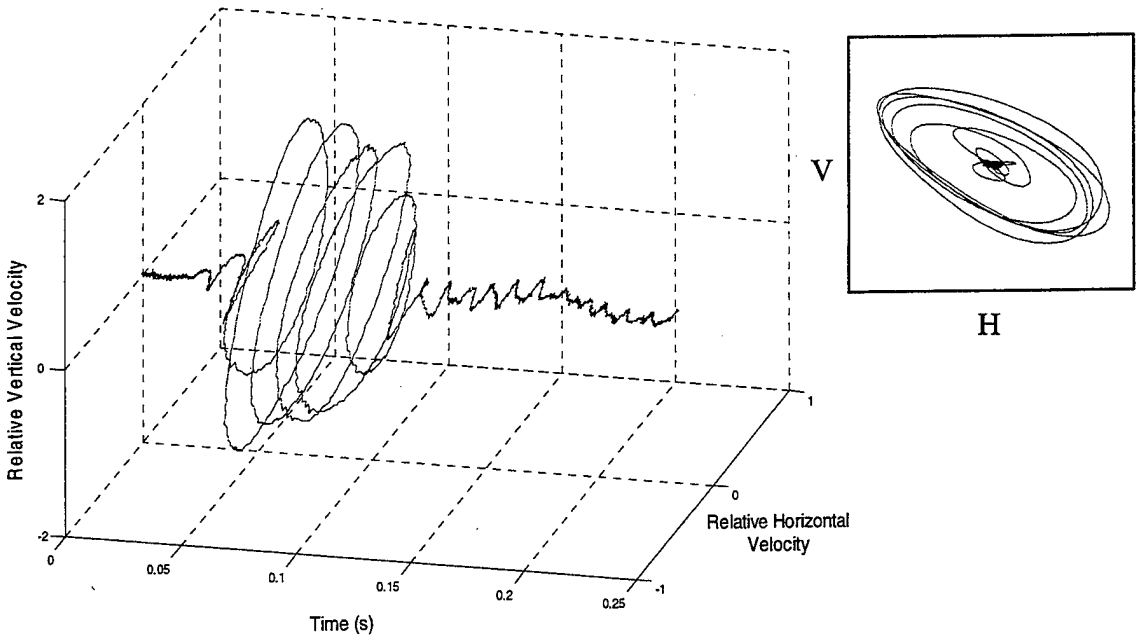

Figure 4.18. . Hankel plot of seismometer velocity signals measured 10 feet (3 m) from array of buried Bass Shaker paddles. Top right plot is the 2-D hodogram Top right plot is the 2-D hodogram (V: vertical, H: horizontal).

It is important to note that the shaker paddles can also be employed vertically. Figure 4.19 shows a sources being emplaced in this fashion. This orientation preferentially excites Love waves (SH type surface waves, see Chapter II) instead of Rayleigh waves. Some experiments were conducted to determine the applicability of Love waves to the seismic sonar and will be discussed briefly in a later section.

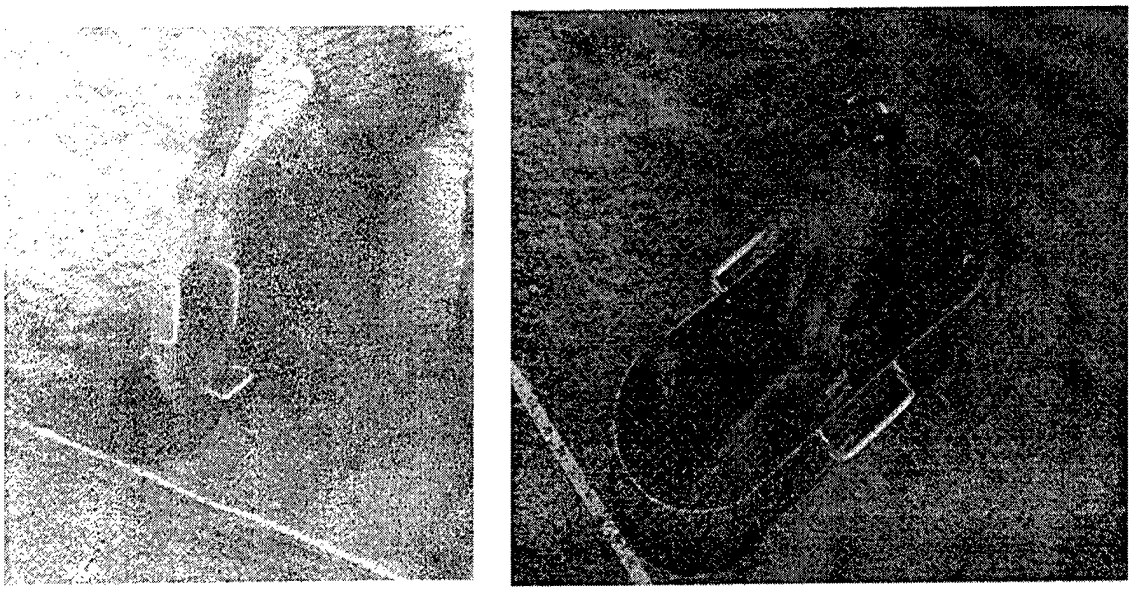

Figure 4.19. Bass Shaker paddle employed with vertical (Love wave) orientation.

THIS PAGE INTENTIONALLY LEFT BLANK

V. FIDUCIAL EXPERIMENTS ON AZIMUTHAL COHERENCE AND BEAMFORMING

As with any sonar system, the purpose of employing an array of sources in the seismic sonar research tool is to form a beam of energy so that the system can maximize energy along a chosen axis and reduce the amount of energy that may scatter from objects off axis. Therefore, before attempting to detect buried objects, it was necessary to conduct preliminary experiments on the feasibility of beam forming in the sand with an array of seismic sources.

A. EXPERIMENT METHODOLOGY

The following experiments were conducted using seismic source(s) in Rayleigh wave orientation (horizontal deployment with vertical excitation). The driver signal waveform for the source was generated by an HP-3314A Function Generator. A single cycle, 100 Hz sinusoidal pulse was generated every second. This pulse was output to the amplifiers that drove the source(s). Each source was driven with 280 watts (rms) during each pulse transmission.

The SPS390 data acquisition system is capable of recording eight channels simultaneously. One of those channels was used to record the driver signal for purposes of triggering. Five of the remaining seven channels were used to record the vertical component of five seismometers. The vertical component alone was sufficient to gain the desired information about the medium's seismic wave propagation characteristics. For both of the following experiments, numerous seismometer positions were required along arcs of a given radius from the source(s). In these cases, five seismometers were employed at a time to record the velocity of the medium in response to the single cycle pulse driven source(s). After each recording, the seismometers were moved to new positions along the arc and the procedure was repeated.

B. AZIMUTHAL COHERENCE

A prerequisite for beam forming in the sand and for sonar signal processing is a reasonable measure of the coherence of propagating signals as a function of angle from a single source. A coherence experiment was conducted using the configuration shown in Figure 5.1.

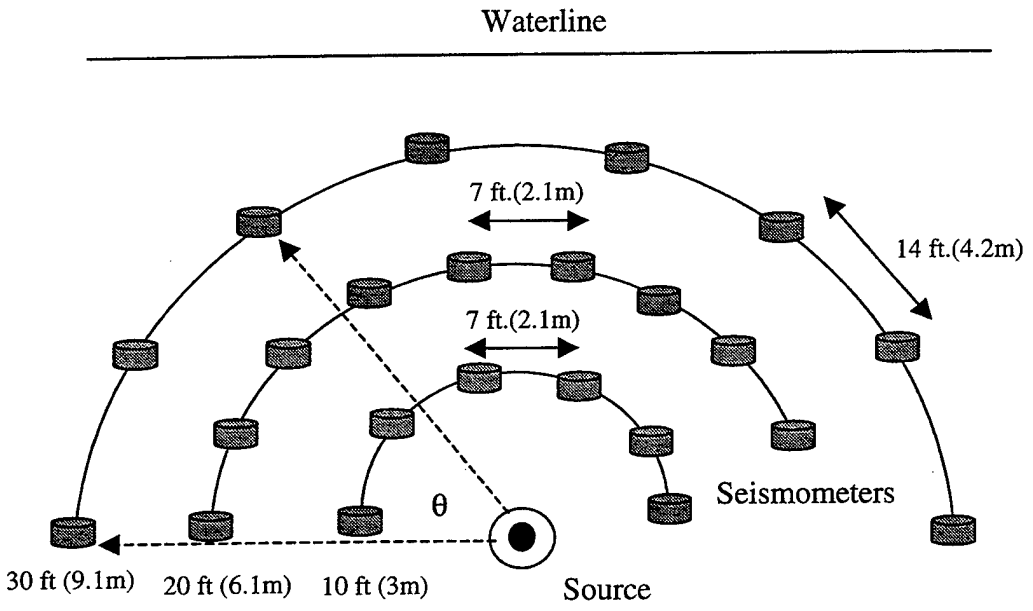

Figure 5.1. Geometry of azimuthal coherence experiment.

Seismometers were placed at uniform intervals along a 180 degree arc at radial distances of 10 ft (3m), 20 ft (6.1m), and 30 ft (6.2m) from the source. For the 10 and 20 ft arcs, the seismometers were spaced at 7 ft (2.1m) intervals, and for the 30 ft arc, at 14 ft (4.2m) intervals. A single source was driven with a single 100 Hz sinusoidal pulse every second. Figure 5.2 shows the driver signal and a sample of two signals received along the 10 ft arc with a separation of 70 degrees.

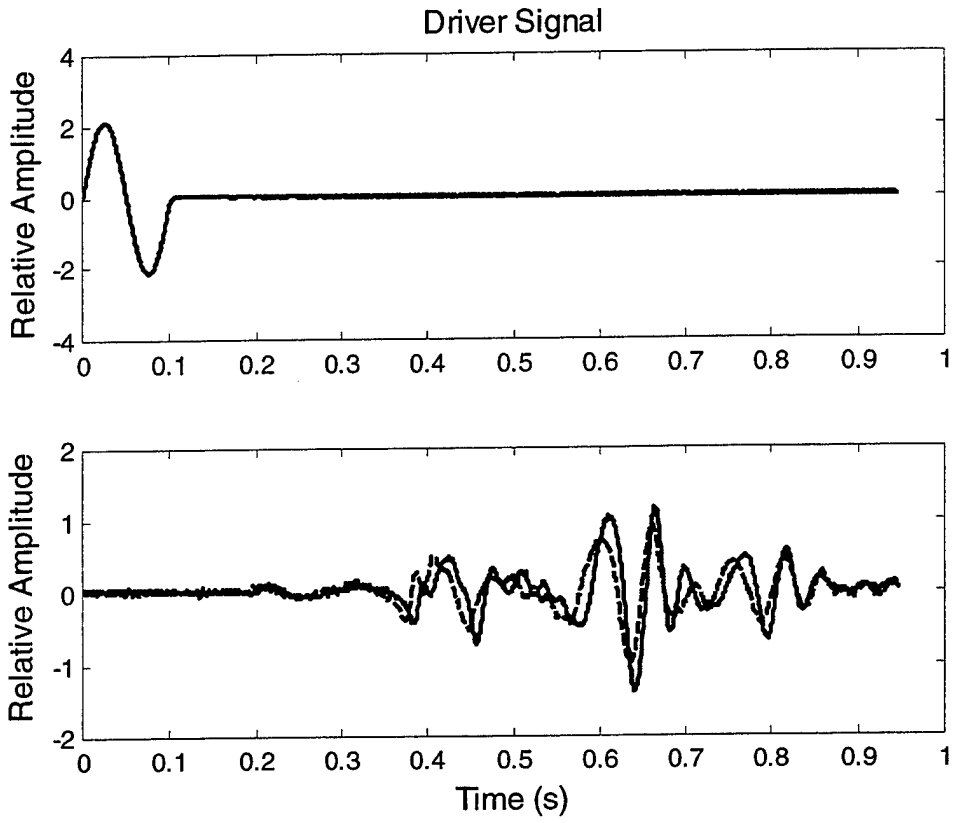

Figure 5.2. Driver and sample received signals from azimuthal coherence test; vertical geophones separated by 70 degrees on a 10 ft (3m) radial arc.

The recorded signal from each seismometer was correlated with every other seismometer in the arc using the correlation coefficient function,

$$\rho_{12} = \frac{C_{12}(\tau)}{\sqrt{C_{11}(0) \cdot C_{22}(0)}}, \tag{5.1}$$

where, $C_{xx}(\tau)$ is the covariance function. At each radial distance, the average correlation was then calculated as a function of angle by taking the mean value of the correlation between each pair of seismometers in the arc that shared a given separation angle. Figure 5.3 shows the resulting average correlation coefficients, as a function of angular separation (θ) between seismometers, at each of the three radial distances. Using 0.7 as a benchmark correlation coefficient for coherent signal processing, these results indicate

that at 10 ft and 20 ft, there is reasonable coherence across 180 degrees, and even on a 30 ft arc, the signals are reasonably coherent to at least 140 degrees separation. Therefore, this "typical" beach environment has requisite spatial coherence to proceed with beamforming experiments.

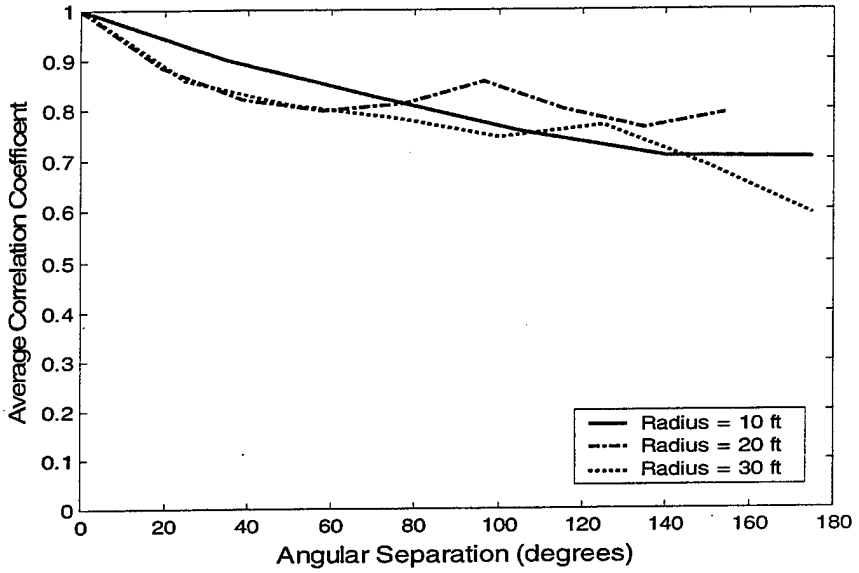

Figure 5.3. Average correlation coefficient as a function of separation angle for ranges of 10 ft (3m), 20 ft (6.1m), and 30 ft (9.1m).

C. BEAM FORMING

The geometry of the beamforming experiment is shown in Figure 5.4. The vertical component of the seismometer signals was recorded at positions along a semi-circle around an array of seven sources. The radius of the arc was 20 ft and the interval between seismometer positions was 1 ft. Figure 5.5 shows a sample of the vertical signals recorded on axis and at 65 degrees off axis. As expected, the amplitude is greater on axis than off axis. The beam pattern was quantified by taking the maximum amplitude of each of the vertical velocity measurements taken along the arc (there were 64 such measurements along the 20 ft arc).

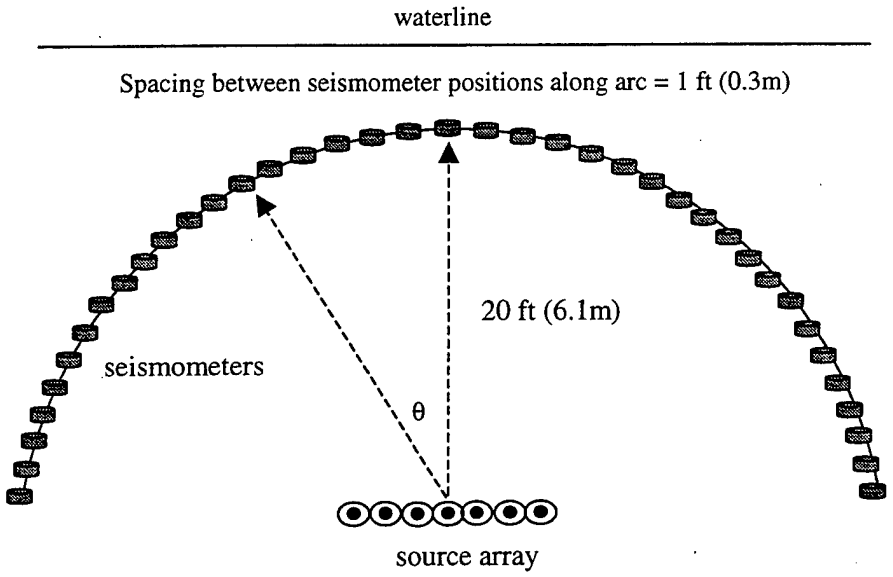

Figure 5.4. Geometry of beamforming experiment.

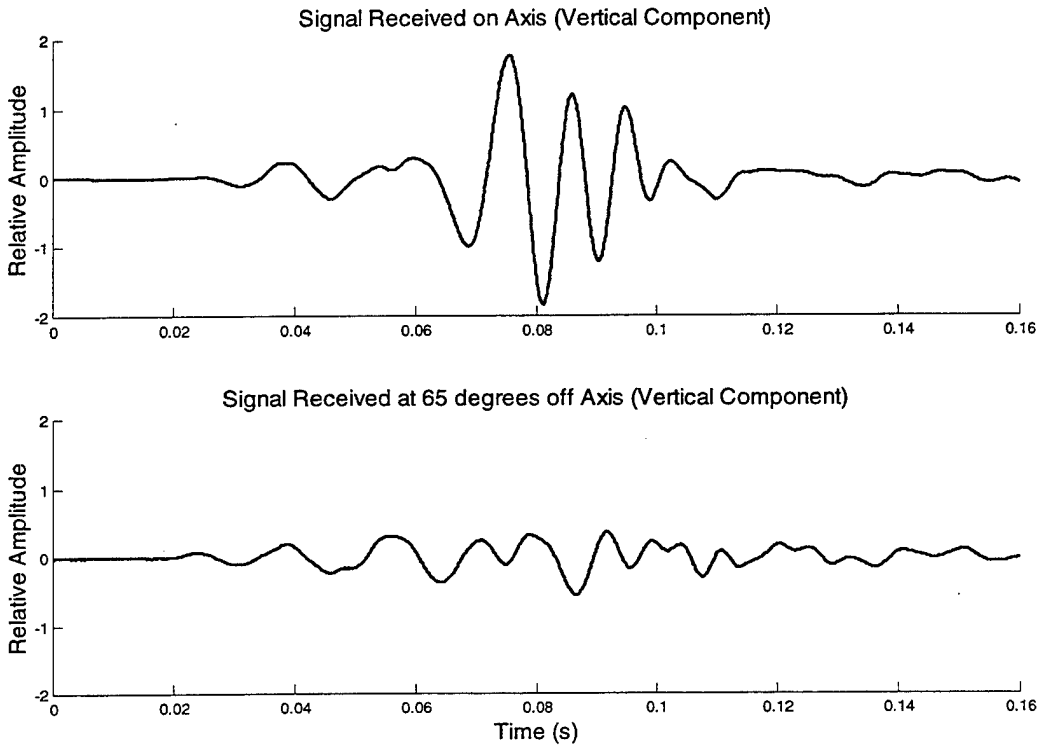

Figure 5.5. Vertical component of recorded signal on axis, and at 65° off axis.

The normalized measured velocity amplitude could then be plotted as a function of angle from the axis using,

$$V_{norm} = 20 \cdot \log \frac{V_m}{V_0}, \tag{5.2}$$

where V_{norm} is the normalized velocity amplitude in dB, V_m is the maximum velocity amplitude measured at the given angle, and V_0 is the normalization factor from the largest amplitude record.

By way of comparison, the theoretical beam pattern was also calculated for a linear array of equally spaced, equally phased, omni-directional sources by plotting the equation ,

$$V_{norm} = 10 \log b(\theta), \qquad where\ b(\theta) = \left[\frac{\sin(n\pi d \sin\theta / \lambda)}{n \sin(\pi d \sin\theta / \lambda)} \right]^2. \tag{5.3}$$

In this acoustic sonar beam pattern formulation [Ref. 25], n is the number of elements, d is the spacing, and λ is the wavelength computed with the driver frequency (100 Hz) and the estimated Rayleigh wave velocity.

Figure 5.6 shows the measured beam pattern plotted against the calculated pattern using seven elements spaced at 14 in (35.6 cm, approximately one-half wavelength) and a Rayleigh wave velocity of 75 m/s. The main lobe of the measured data matches the calculated lobe quite well using this Rayleigh wave velocity. The half-power angle, θ_{hp}, (measured at –3dB) for the measured pattern is 7.6 degrees. At a range of 20 ft (6.1m), this angle gives a beam width of 5.3 ft (1.6m). At a range of 15 ft (4.6m), which is the target range used in the following sections, this angle corresponds to a main lobe width of 4 ft (1.2m).

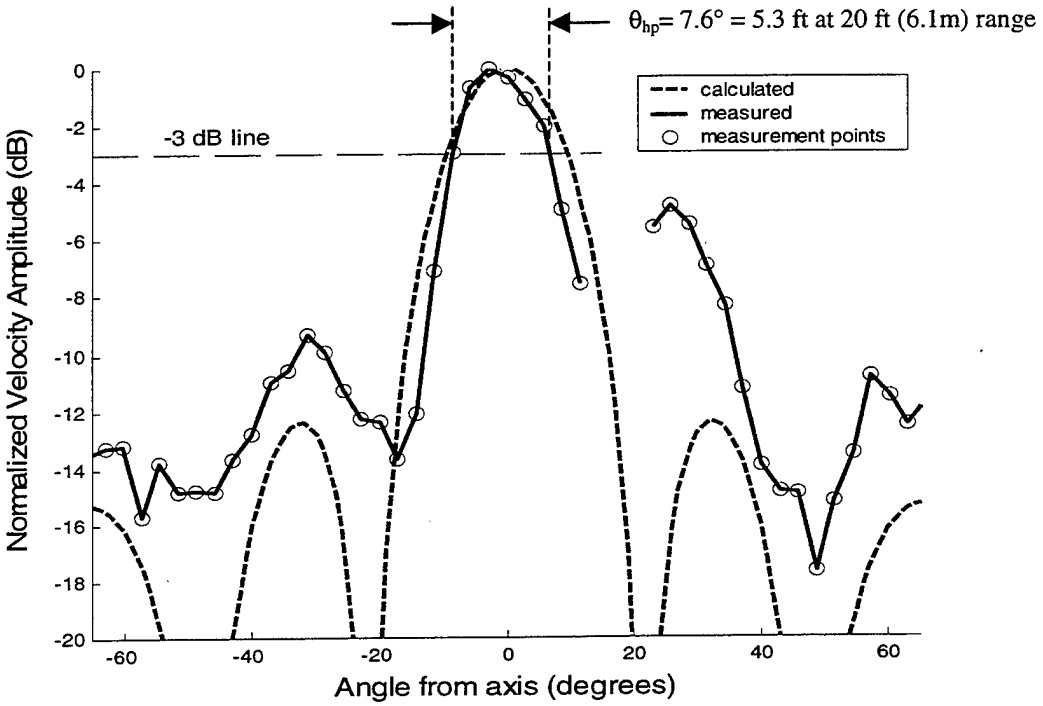

Figure 5.6. Measured (vertical velocity component) and calculated beam pattern at 20 ft (6.1m) range for seven equally spaced, omni-directional elements , driven at uniform amplitude and phase.

The slight leftward skew of the measured main lobe is not significant, as it may easily be due to positioning errors made on the beach, where distance measurements were made by hand. The raised sidelobe on the right side of the measured plot is due to an experimental error that has not been determined.

THIS PAGE INTENTIONALLY LEFT BLANK

VI. TARGET DETECTION

The baseline experiments presented above provide promising results in regard to using an array of seismic sources to form a coherent seismic sonar beam in the sandy medium of the beach experiment site. The following sections describe how the target detection experiments were conducted and what signal processing methods were used to extract target echoes from the recorded data. Finally, the detection results of a Mk-63 naval mine and a M-19 anti-tank mine, both completely buried, are presented and discussed.

A. EXPERIMENT METHODOLOGY

1. Array Configuration

Upon deploying the seismic sonar research tool to the beach experimental site, there were a number of ways to configure the source and receiver arrays with respect to the target. Future implementations will easily enable the system to electronically steer the seismic sonar beam in real time, however, the present research tool was mechanically steered for reasons of simplicity. Generally, one can consider two basic configurations for the seismic sonar, mono-static and bi-static. Figure 6.1 shows a simple diagram illustrating how these configurations differ. At the beginning of target detection experiments, both of these configurations were used to determine which would be most favorable for the seismic sonar. It was determined that bi-static is an advantageous configuration because the seismometer array is off the axis of the source array, and the direct blast from the transmitters is much less intense. Because the target echo in these experiments arrives at the seismometer array only a fraction of a second after the direct blast, it was useful to minimize that blast so that the seismometers could sufficiently "relax" (vibrationally) before the echo arrives. This is only applicable for the present experiments. In subsequent utilizations with longer range seismic sonars, the seismometer relaxation time will be of no consequence.

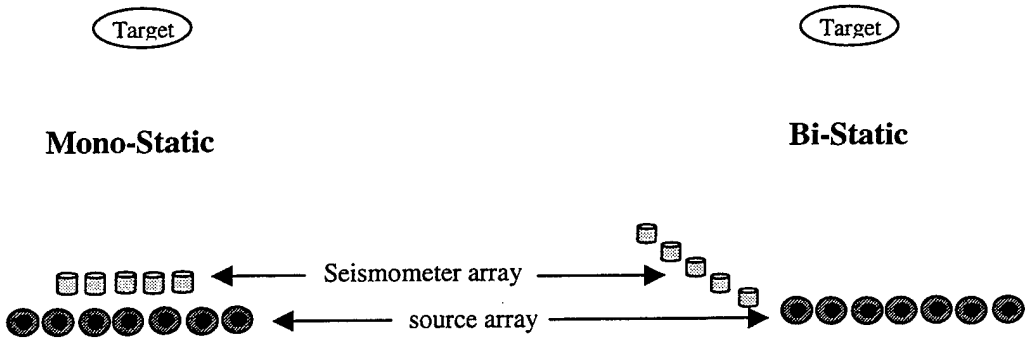

Figure 6.1. General mono-static and bi-static array configurations.

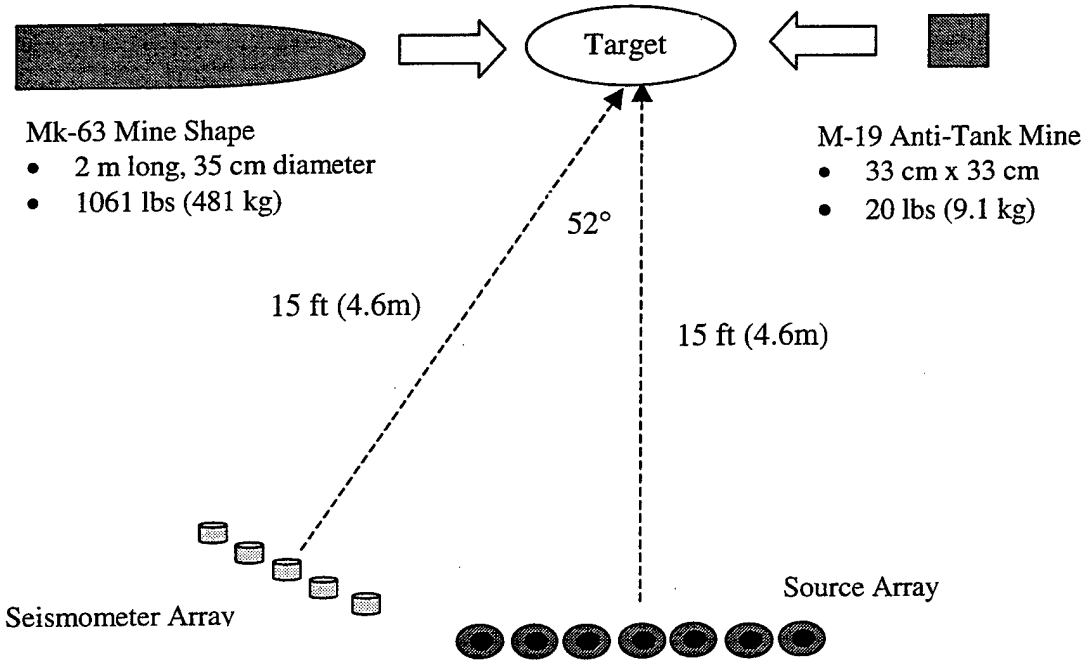

Figure 6.2. Bi-Static configuration used for detection experiments for Mk-63 mine shape and M-19 anti-tank mine.

The bi-static configuration [Ref 26] shown in Figure 6.2 was used for all of the target detection experiments presented in this thesis. The seismic source array, with seven elements separated by a half wavelength, was about 8 ft (2.4m) long and the five-seismometer array, also spaced at a half wavelength was about 6 ft (1.8m) long. The targets were placed on the main beam axis to both arrays, at a distance of 15 ft (4.6m).

As mentioned in the section on source development in Chapter IV, the current paddle design can be employed so that the paddle is oriented horizontally (and the vibration motion is vertical) to obtain Rayleigh wave motion at the target, or vertically (so that the vibration motion is horizontal) to excite horizontally polarized shear surface waves known as Love waves. This thesis focuses on using Rayleigh waves in order to utilize the advantages of vector polarization filtering, but some preliminary results of recording the echo returns from Love waves are presented in a later section.

2. Target Emplacement

Figure 6.3 shows the targets available for this research. Highlighted are the targets used in the experiments presented in this thesis. The Mk-63 mine shape is an inert, Mk-83 general purpose 1000 lb steel bomb equipped with mine fusing mechanisms. The Mk-63 is 2 m long and 35 cm in diameter and has an actual weight of 1061 lbs (481 kg). The M-19 is a square, non-metallic, blast type anti-tank mine. This plastic mine is 33 cm x 33cm x 7.5 cm and weighs 20 lbs (9.1 kg).

Deploying the Mk-63 mine shape was a challenge. A carrier trailer, equipped with a 4000 lb winch and other hoist and slide apparatus, enabled the 1000 lb bomb to be transported to the beach, and placed on the ground. Once the mine was on the beach, a hole was dug next to it, and the mine was rolled into the hole and then buried. Figure 6.4 shows a picture of how the mine was removed from the trailer (left) and a picture of the mine in place just prior to burial (right). The M-19 mine could be emplaced by hand and is shown prior to burial in Figure 6.5. All targets were buried so that the top surface could be covered nearly flush with the surrounding sand.

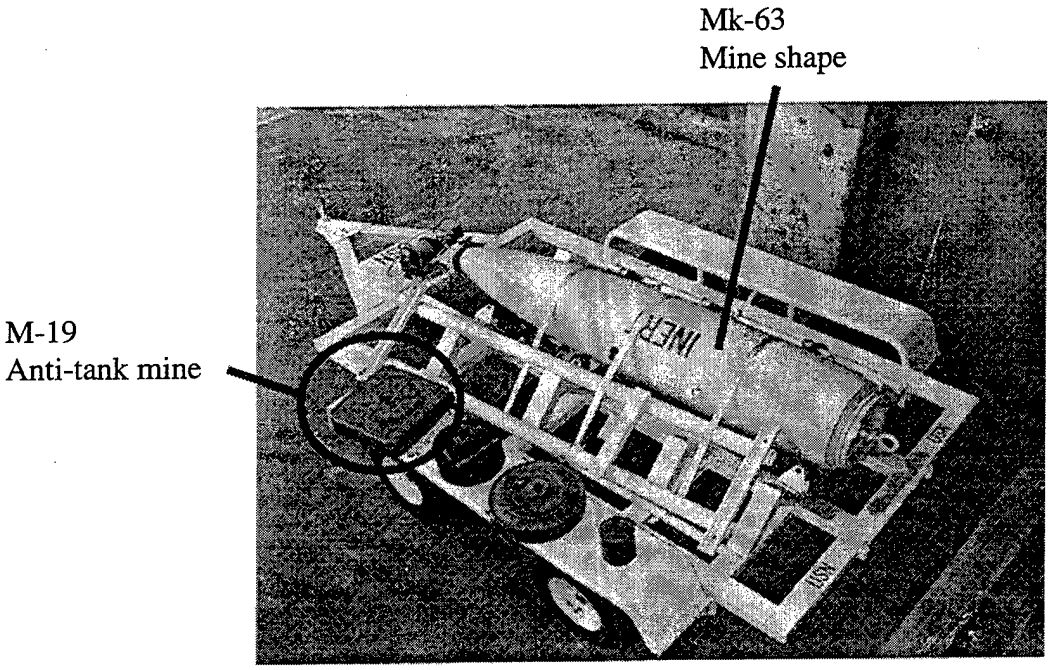

Figure 6.3. Target mines and ordnance.

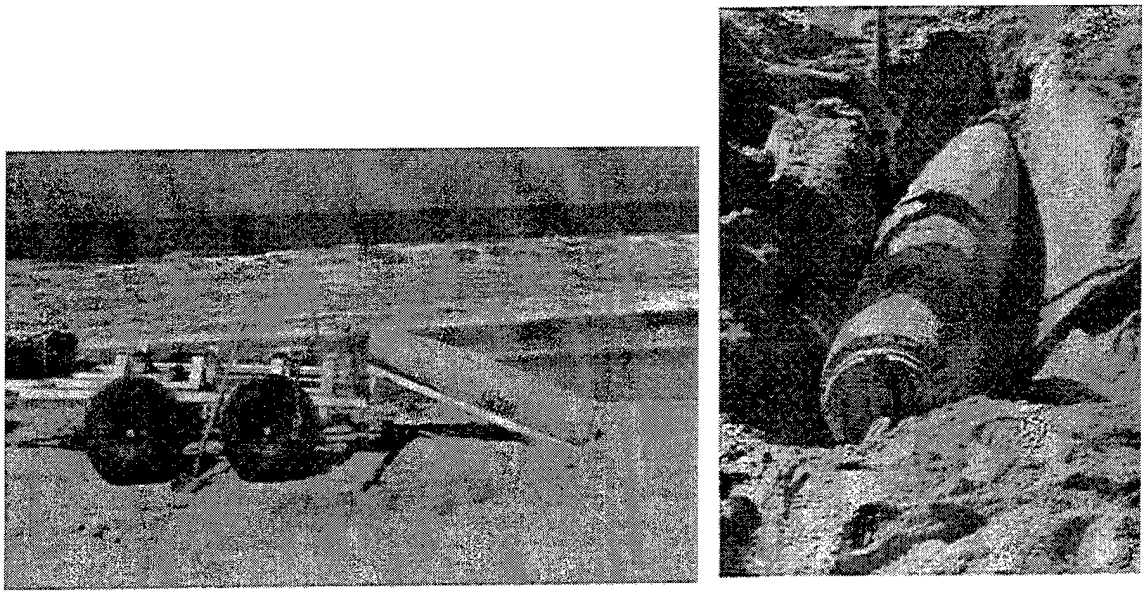

Figure 6.4. Pictures taken during the Mk-63 mine shape emplacement procedure, at low tide, showing the surf zone of Monterey Bay in the background.

Figure 6.5. Picture of the M-19 anti-tank mine prior to complete burial.

3. Data Collection

For target detection experiments the driver signal was identical to that used in the experiments discussed in Chapter V (1 cycle/pulse transmission, centered at 100 Hz). The seismometer signals were band pass filtered between 30-300 Hz and amplified (x100) using Ithaco 120 Low Noise Preamplifiers. Target detection using Rayleigh waves requires that both the vertical and radial components of the seismometers be recorded so that one can use the signal processing methods (described in a later section) to isolate the target echo. In the few target detection experiments conducted using Love waves, only the transverse component was recorded because the preferentially excited motion was due to horizontally polarized shear waves (SH waves).

The first step in all of the target detection experiments was to record a data set without a target in place. This provided a means to establish the medium's intrinsic

response to the source array vibration. Even in the bi-static configuration, a major portion of the source array energy is recorded by the seismometer array. This "direct blast" will exist with or without the presence of a target and can be removed as common signal during the coherent subtraction process described in the following section. Once the "no target" data was recorded, the target was placed in the ground at an on-axis distance of 15 ft from both arrays.

B. SIGNAL DESIGN AND PROCESSING

There are three signal processing techniques that were used in this research; beam construction, coherent subtraction and vector polarization filtering. Used together, these techniques provide a powerful means to extract the target echo from extraneous body wave signals and reverberations.

1. Receiver Beam Construction

In Chapter V, the results of the source array beam forming experiments were discussed. Here, the seismometers recorded the superposition of the waveforms generated from all of the sources. For target detection experiments, the target is placed on the source array axis where seismic wave energy will be maximized. The individual seismometers in the receiver array, however, will record the ground or seafloor particle velocity from waves coming from all directions. Therefore, in order to maximize the signal approaching the receiver array on axis, while minimizing the signals approaching from off axis, the coherent summation of the individual seismometer records was performed as a initial step in the signal processing effort. This was done by simply adding (using MATLAB) the recorded time traces from each seismometer in the following way,

$$v_t(t) = \sum_{n=1}^{m} v_{sn}(t), \tag{6.1}$$

where $v_t(t)$ is the total "beam formed" seismometer array signal, $v_{sn}(t)$ is the signal from the n^{th} seismometer, and m is the total number of seismometers in the array. Note that this coherent summation was done individually for each recorded seismometer component. Because the signals arriving on axis will have the least seismic wave path difference to the individual seismometers, the signals will add in phase, whereas the off-axis signals will have more significant path differences and add out of phase causing "destructive interference".

2. Coherent Subtraction

Coherent subtraction or "background subtraction" is very simply the time-domain subtraction of "beam formed" seismometer signals without target from the corresponding signals with a target present. As mentioned above, this technique reduces the signal to one which is generated by changes to the medium (target emplacement) between recordings. The coherent subtraction is a simple process in MATLAB which can be expressed as,

$$v_{i/CS}(t) = v_{i/T}(t) - v_{i/NT}(t), \tag{6.2}$$

where i is each of the three recorded velocity components (vertical, radial or tangential). Here, $v_{i/cs}(t)$ is the coherently subtracted signal for a given component, $v_{i/T}(t)$ is the recorded signal for a given component with the target buried, and $v_{i/NT}(t)$ is the recorded signal for a given component with no target buried.

3. Vector Polarization Filtering

As discussed in Chapters II and IV, Rayleigh waves, have a vertical component that lags the radial component by 90 degrees, such that the resulting particle motion is elliptical. Rayleigh waves are thus vector wave fields rather than the scalar wave fields that describe acoustic waves. Vector polarization filtering provides a method of extracting the Rayleigh waves in a seismic recording from the unwanted body waves (P

and S waves) that may have reflected from a deep, complex substructure. This filtering is done digitally in MATLAB by applying the Hilbert Transform to the radial and vertical signals, and calculating the complex power function given by,

$$P_{r,v}(t) = V_r^*(t) x V_v(t), \tag{6.3}$$

where $P_{r,v}(t)$ is the complex power function, $V_r(t)$ and $V_v(t)$ are the complex signals obtained from the Hilbert Transform of the received (real) radial and vertical signals, and V* denotes complex conjugation. [Ref. 11] Figure 6.6 shows graphically how the phase relationship between the vertical and radial velocity provides the Rayleigh wave with an imaginary component in the complex power, while the P-wave (acoustic) noise, with in phase components, yields a real component in the complex power. As will be shown in the following section, one can plot the imaginary component of the complex power as a function of time to isolate Rayleigh wave reflections from buried objects.

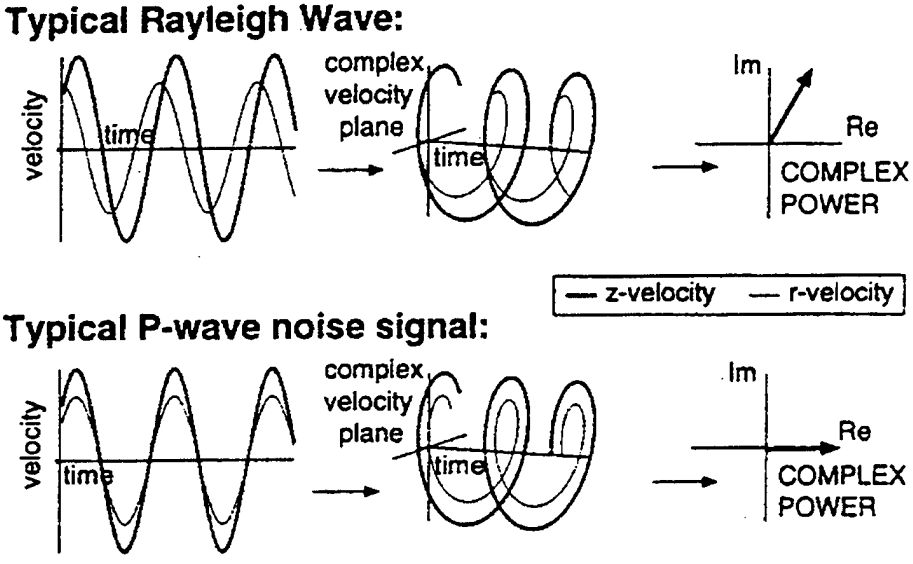

Figure 6.6. Principles of vector vs. scalar wave velocity and complex power relations. From Ref. [11].

C. RESULTS

1. Mk-63 Mine Shape

The Mk-63 mine shape was the largest target used in this research. (see Figure 6.3) Several experiments were conducted with Rayleigh waves to detect the Mk-63. Some preliminary experiments were conducted with Love waves (see section 3 of this chapter), but they were not conclusive and were deemed to require further research and development.

For Rayleigh wave target detection experiments, the shaker paddles were oriented horizontally as shown in Figure 4.17. The additional tool of vector polarization filtering allows one to look not only at the seismometer particle velocity components as a function of time, but also at the imaginary component of the complex power. The top two traces of Figure 6.7 show a plot of the radial and vertical components of particle velocity as a function of time with and without the Mk-63 mine shape which was buried at a range of 15 ft (4.6m). Additionally, the bottom trace shows the imaginary component of the complex power calculated using the vertical and radial components with and without the mine shape target. It is important to note that no coherent subtraction has been done for this figure. The complex power is simply calculated separately for the data with and without the buried target. The large arrival that is common to both the "with target" and "without target" data is the direct blast across the seismometer array. This direct blast lasts for about 0.09 seconds and can be considered a constant of the system/medium interaction. This direct blast introduces a "minimum range" for the seismic sonar, and for Rayleigh waves with an estimated speed of 75 m/s, this minimum range is about 13 ft (4m).

The imaginary component of the complex power becomes even more pronounced if the radial and vertical components with and without target are coherently subtracted *before* the complex power is computed. Figure 6.8 shows a plot of the imaginary

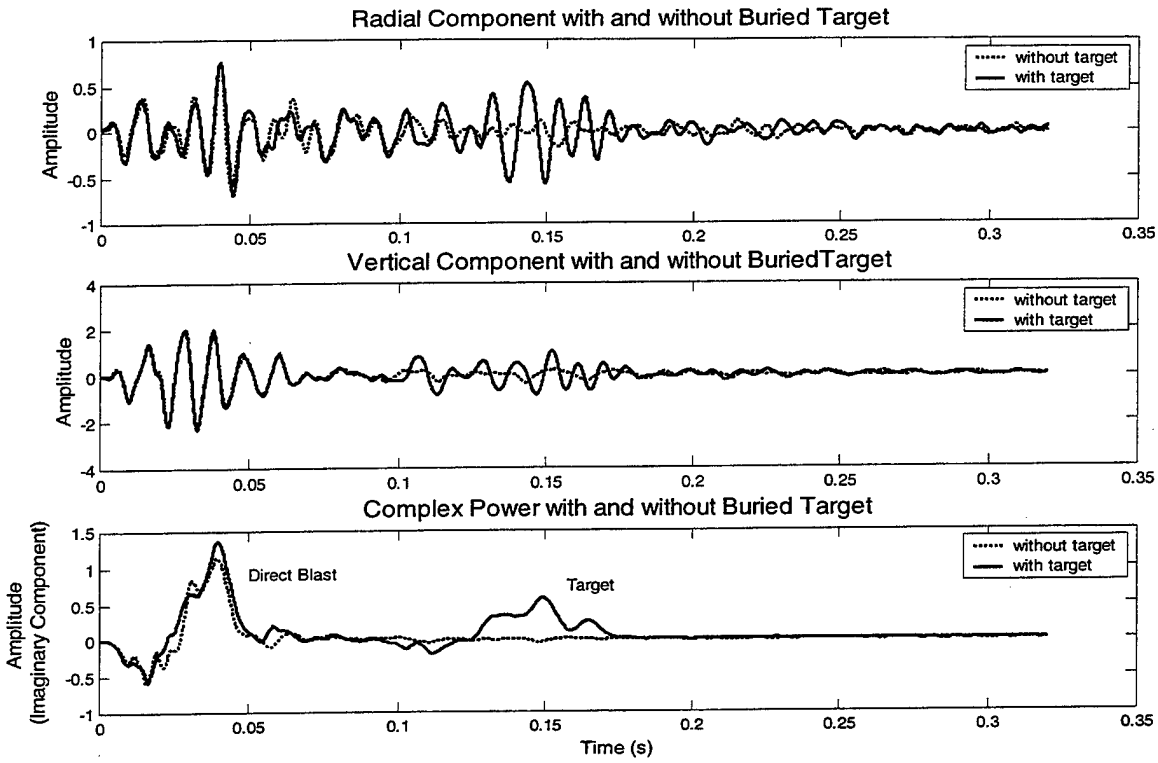

Figure 6.7. Data (before coherent subtraction) for buried Mk-63. Range = 15ft (4.6m).

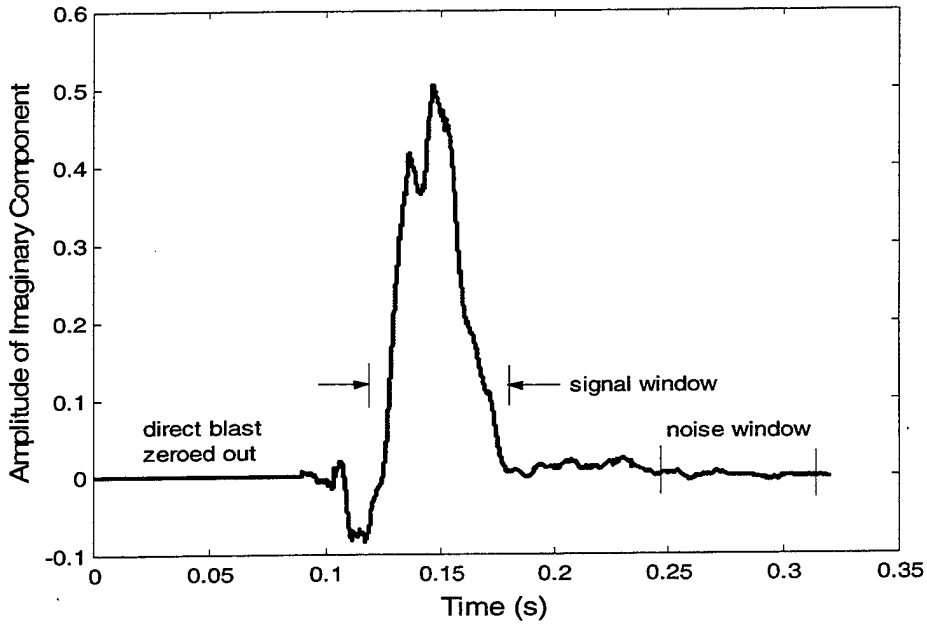

Figure 6.8. Imaginary component of component of complex power after coherent subtraction. Mk-63 target at a range of 15 ft (4.6m).

component of the complex power after coherently subtracting the radial and vertical signals shown in the top two traces of Figure 6.7. Note that the initial blast portion of the trace is not important and has been zeroed out. The signal to noise (S/N) ratio of the target echo was computed in two different ways; peak signal to RMS noise and RMS signal to RMS noise. The windows used for the RMS calculations are shown on the figure. The peak signal to RMS noise yields a S/N ratio of 23 dB. The RMS signal to RMS noise yields a S/N ratio of 21 dB. These high signal to noise ratios are a significant advancement in detecting buried mines with seismic sonar. With target returns of this magnitude, the seismic sonar operating range can conceptually extend from current experimental ranges of 4-5 meters to ranges of a few tens of meters. The ability to operate from such a distance would be an enormous stride toward solving the problem of buried mine detection.

An interesting feature of the imaginary component of the complex power is the deflection direction. A positive deflection indicates prograde particle motion and a negative deflection indicates retrograde particle motion. [Ref. 27]. In Figure 6.8, there is a small negative deflection followed by a large positive deflection. Most of the discussion of Rayleigh waves to this point has indicated that the particle motion at the surface is retrograde elliptical. However, as shown in Figure 2.2, at a depth of roughly 0.1λ, the particle motion switches from retrograde to prograde, and remains prograde until the motion decays to an insignificant level at roughly 2λ. For this experiment, the depth for this polarity switch is about 3 in (7.6 cm). The Mk-63 mine shape has a vertical cross section of 15 in (38 cm) so when buried flush with the surface, 80% of the target lies below this polarity crossover point. This may be the reason why the deflection indicated predominantly prograde motion.

Another way to present the information contained in the return signal after vector polarization filtering is to plot a spectrogram of the energy contained in the imaginary part of the complex power. Figure 6.9 shows a grayscale spectrogram of the imaginary part of the complex power after coherent subtraction of the signals recorded with and without the Mk-63 mine shape buried at 15 ft. This plot displays the (normalized) energy in the signal over a range of frequencies as a function of time. The darker regions

indicate greater energy. Note that, because signals were coherently subtracted, there is no energy corresponding to the direct blast. However, at about 0.125 seconds there is energy centered around 100 Hz, corresponding to the echo return from the Mk-63 mine. This method of analyzing the data could possibly lead to classification clues in future developments of this research. Harmonics in the echo return may provide information to distinguish man-made from natural buried objects. This might be the case, for example, if a natural target, such as an irregular shaped rock, did not provide coherent reflectivity at all the harmonic frequencies. However, this technique was not developed in this thesis and is presented here only to indicate a potential tool for future research.

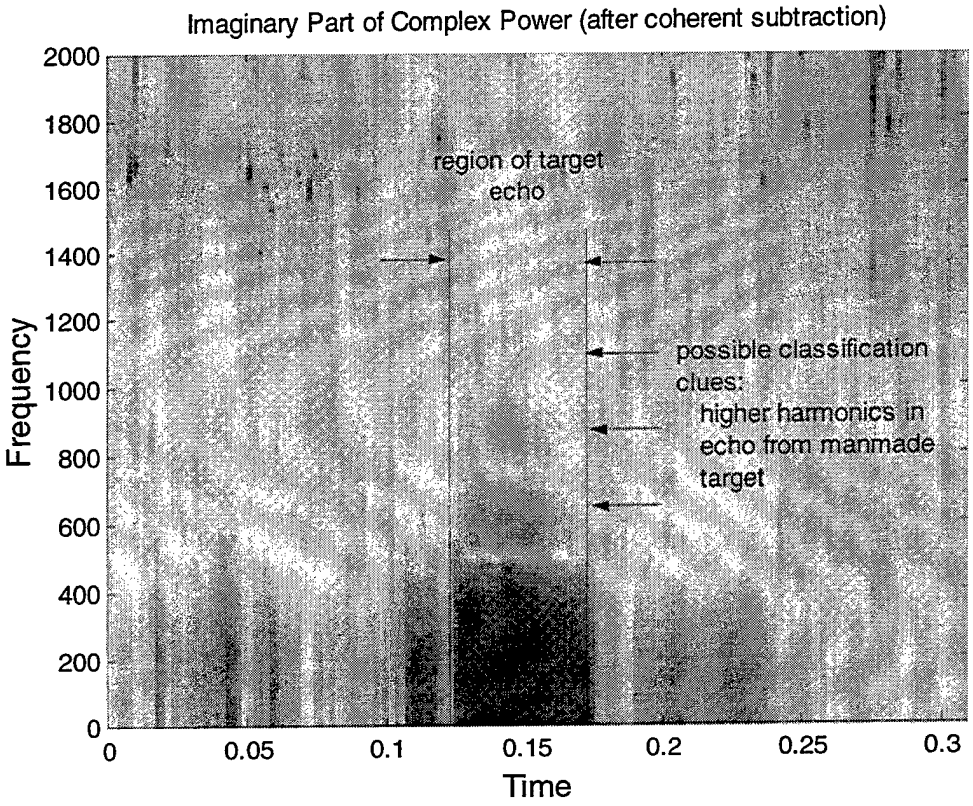

Figure 6.9. Spectrograms of the imaginary part of the complex power, after coherent subtraction, with the Mk-63 buried at a range of 15 feet (4.6m).

2. M-19 Anti-Tank Mine

The M-19 anti-tank mine is significantly smaller than the Mk-63 mine shape and the amplitude of the target echoes were not as strong. The M-19 target echo was only discernable upon plotting the imaginary part of the complex power *after* coherent subtraction, as done in Figure 6.8 for the Mk-63 mine shape. Figure 6.10 shows the amplitude of the imaginary part of the complex power as a function of time (with the direct blast zeroed out) using the coherently subtracted radial and vertical seismometer components recorded with and without the M-19 mine emplaced at a range of 15 ft (4.6m).

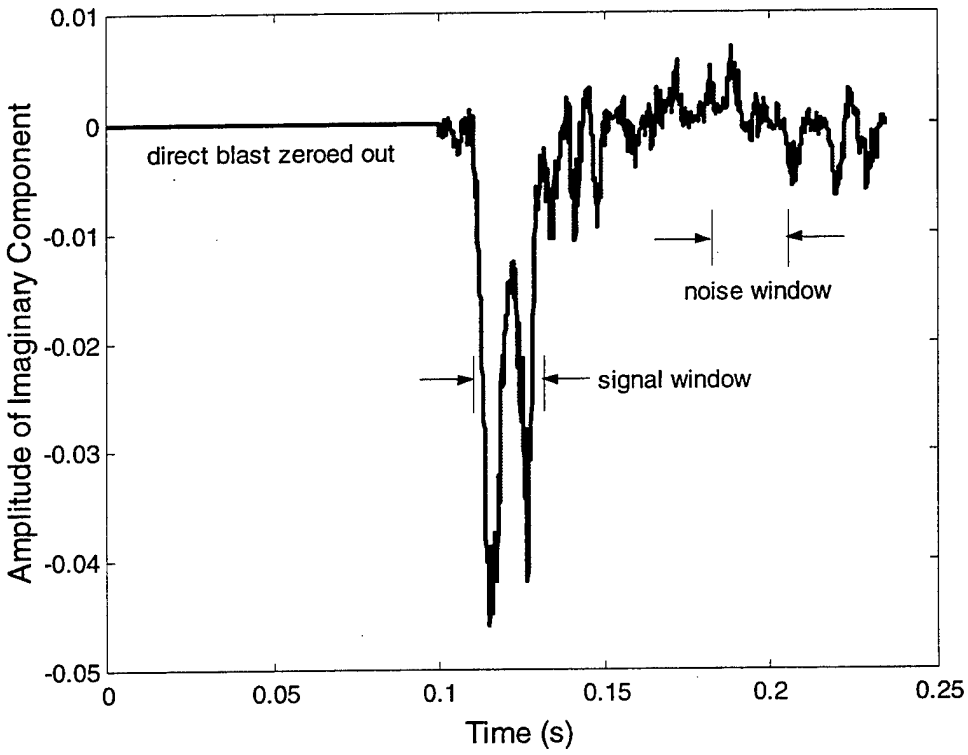

Figure 6.10. Imaginary component of component of complex power after coherent subtraction. M-19 anti-tank mine at a range of 15 ft (4.6m).

Note that while the scale is significantly smaller than that of Figure 6.8, there is an arrival that is distinctly above the noise level, that begins at about 0.11 seconds. As in the Mk-63 data, this time corresponds to a calculated roundtrip time for a Rayleigh wave reflecting from an object 15 ft (4.6m) away. In this case, the peak signal to RMS noise yields a S/N ratio of 12 dB, and The RMS signal to RMS noise yields a S/N ratio of 9 dB. These values are less than that of the much larger Mk-63 mine shape as expected, but indicate a very significant ability to detect small buried mines.

For the Mk-63 mine shape, the positive arrival in the complex power was hypothesized to be due to the fact that 80% of the target was below the depth of polarity reversal for the Rayleigh wave particle motion. Interestingly, the complex power deflects only negatively for the M-19 mine corresponding to predominantly retrograde motion. This may support the above hypothesis because the M-19 has a vertical cross section thickness of only 3.25 in (8.3cm). This corresponds to less than 10% of the target lying below the polarity reversal depth.

3. Detection Using Love Waves

As discussed in Chapter IV, the source paddles can be buried vertically to excite horizontally polarized Love waves. To assess the applicability of using Loves waves for buried mine detection, a preliminary experiment was conducted to determine if there was a significant arrival in the transverse component of the seismometer signal corresponding to a reflected Love wave. Figure 6.11 shows a plot of the transverse component of particle velocity as a function of time with and without the Mk-63 mine shape buried at a range of 15 ft (4.6m), and the resulting coherent subtraction of these signals. The arrival in the "large target" trace corresponds to the echo return of a transverse wave (Love wave) travelling at 83 m/s.

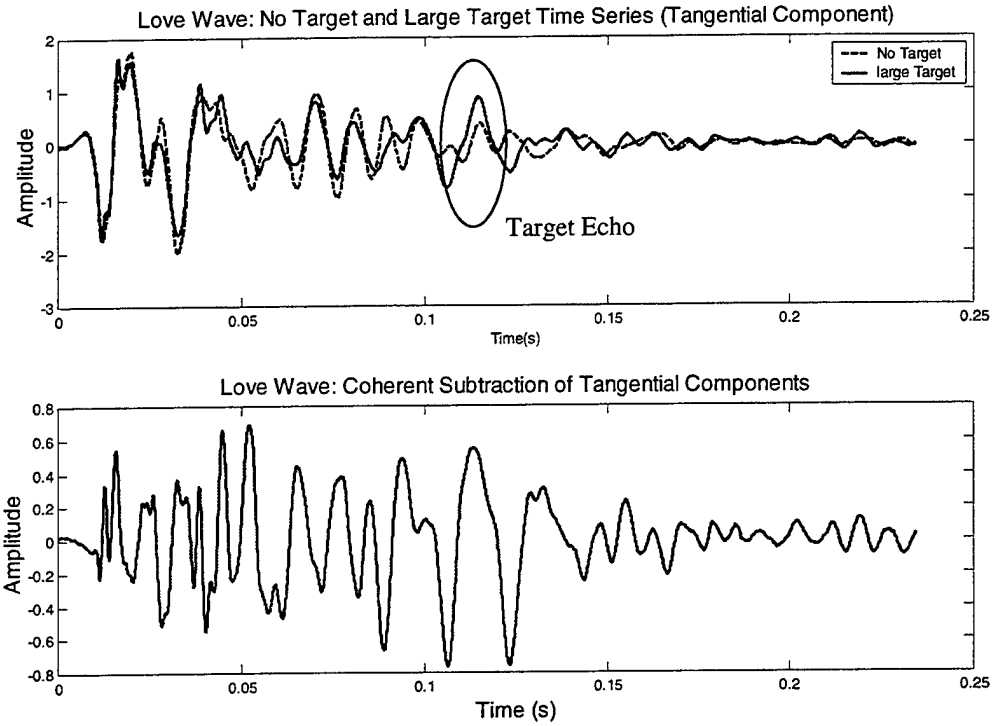

Figure 6.11. (Top) Time series of transverse component of seismometer signal with and without Mk-63 target buried at a range of 15 ft (4.6m). (Bottom) Coherent subtraction of time signals in top trace.

An attempt to detect the M-19 anti tank mine is shown in Figure 6.12. Here, an arrival attributable to a target reflection is not distinguishable. Even after coherent subtraction, there were no identifiable target echoes. Interestingly, other experiments show that the Love wave array configuration produced strong transverse energy at distances out to 40 ft (12.2m) from the source array.

Research for this thesis concentrated on using Rayleigh waves and very little time was spent investigating the potential for utilizing Love waves in seismic sonar. Love waves still may provide an important tool for seismic sonar in some environments, but more research is required to model and understand Love wave propagation and scattering characteristics. This is an important topic for subsequent student thesis projects.

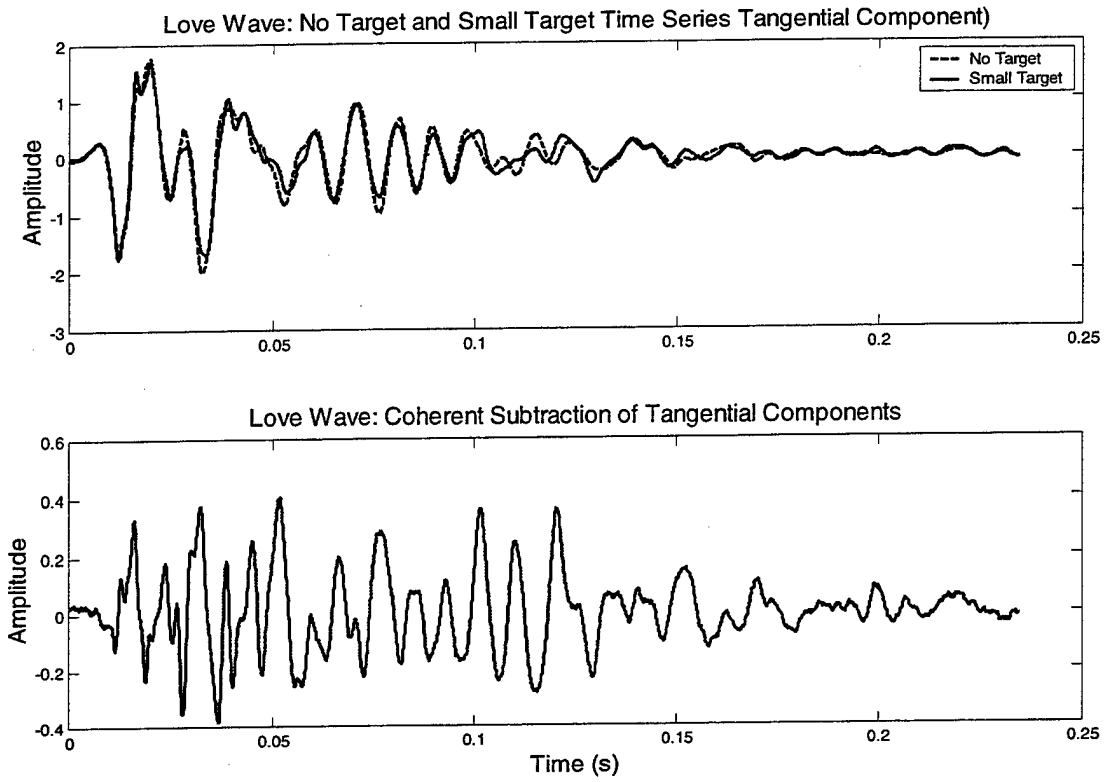

Figure 6.12. (Top) Time series of transverse component of seismometer signal with and without Mk-19 target buried at a range of 15 ft (4.6m). (Bottom) Coherent subtraction of time signals in top trace.

VII. CONCLUSIONS AND RECOMMENDATIONS

Buried land and naval mines continue to disrupt U.S. capability to project naval power ashore and conduct land warfare operations. These disruptions only serve to increase the chance of inflicting casualties on American soldiers, sailors, and marines. This research has taken significant steps toward solving the enormous problem of detecting buried mines quickly and safely.

The goal of this thesis was to advance the capabilities of seismic sonar by improving the surface wave sources and investigating the ability to employ an array of such sources as part of a seismic sonar research tool. A significant amount work went into designing and building a system that was capable of deploying all of the necessary power and electronic equipment directly to the field environment to conduct realistic experiments. The results of these efforts were depicted in Figures 4.4, 4.5, and 4.6.

A new source design of dual Bass Shakers mounted to a circular plate (see Figure 4.16) shows promising results with excellent Rayleigh wave particle motion in the far field. Furthermore, field experiments successfully demonstrated the ability to employ these new sources in a linear array and to form a beam of seismic surface wave energy in the realistic sandy medium at the Naval Postgraduate School beach.

Through signal processing techniques such as coherent subtraction and vector polarization filtering, the seismic sonar was able to successfully detect a Mk-63 mine shape and a M-19 anti-tank mine. Impressive signal to noise ratios of 23 dB for the Mk-63 and 12 dB for the M-19 were achieved from experiments employing the arrays in a bi-static configuration with the target buried just beneath the beach surface at a range of 15 ft (4.6m). The ability to detect the small (33cm x 33cm x 7.5 cm) anti-tank mine with this signal to noise ratio is a breakthrough for this ongoing seismic sonar project and the options for future research, development and implementation are many.

For purposes of experimental simplicity, this research was conducted on the beach where surface waves, known as Rayleigh waves, were generated along an air-sediment boundary. However, as mentioned in Chapter II, surface waves with the same characteristics, known as Scholte waves, can be generated along a water-sediment

interface. Therefore, with sea worthy source and receiver arrays, the seismic sonar should function equally as well in the shallow surf zone. Moving the experiments seaward is an important next step in seismic sonar research for Navy and Marine Corps applications.

Source improvement continues to play an important role as different configurations may be developed to improve sediment coupling or to operate over a greater frequency range. The sources used for this study were optimized for a 100 Hz driver signal and the need to increase the frequency and bandwidth for signal processing options is paramount. Target classification is another key area for future research. Classification and false target rejection schemes such as frequency domain resonance detection, or, as mentioned above, high frequency imaging to estimate target size and shape, must be developed to distinguish man made from natural targets.

Finally, the seismic sonar is being developed to solve a major problem facing the U.S. Army, Navy and Marine Corps, and thus must be "militarized" to accommodate practical deployment methods for service use. The system clearly lends itself to robotic platforms and the future lies in research to develop such platforms to acquire and process data in real time. With the further development of range capability for seismic mine countermeasures sonar, it is entirely possible that manned platforms such as ships and amphibious craft of the fleet, as well as combat vehicles of the Marine Corps and the Army, can be equipped to detect and classify buried mines at safe stand-off ranges.

APPENDIX A. MANUFACTURER SPECIFICATIONS FOR SM-6 AND SM-11 GEOPHONES

INPUT OUTPUT, INC.

SENSOR Nederland bv

SM-6 Geophone

- Long travel version of the SM-4 8 Hz, 10 Hz and 14 Hz geophone, also available in 4.5 Hz natural frequency
- Special orientations on request beyond the normal vertical and horizontal options
- Widely used in industrial vibration monitoring systems
- Rugged construction with precious metal rotating coil contacts
- 2 year warranty

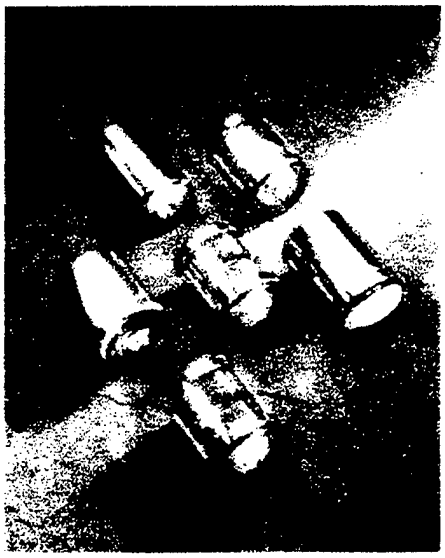

The SM-6 geophone is a long coil travel version of the time proven SM-4 geophone. The extra coil travel offers an advantage for higher tilt requirements and where larger amplitude signals may be encountered, for example in industrial vibration monitoring. A range of natural frequencies is available from 4.5 Hz to 14 Hz, providing choice of the correct geophone for a wide variety of applications.

The SM-6 can be supplied for vertical and horizontal orientation, other specialized versions are available on request, for example Galperin (54.7 deg.), 45 deg.

The SM-6 is an ideal choice for the shear wave horizontal elements partnering an SM-4 vertical geophone in a 3-component package.

A variety of I/O Sensor land cases can accommodate SM-6 geophone elements, making them suitable for an extensive range of field applications.

Specifications (cont.)

SM-6 LOW FREQUENCY GEOPHONE	A-Coil	B-Coil
Frequency		
Natural frequency	4.5 Hz	4.5 Hz
Tolerance	± 0.5 Hz	± 0.5 Hz
Maximum tilt angle for specified Fn	0	0
Typical spurious frequency	140 Hz	140 Hz
Distortion		
Distortion with 0.7 ips p.p. coil to case velocity	< 0.3%	< 0.3%
Distortion measurement frequency	12 Hz	12 Hz
Maximum tilt angle for distortion specification	0	0
Damping		
Open circuit damping	0.265	0.56
Open circuit damping tolerance	+/- 5%	+/- 5%
Resistance		
Standard coil resistance	375 Ω	375 Ω
Tolerance	± 5%	± 5%
Sensitivity		
Open circuit sensitivity	28.0 V/m/s (0.71 V/in/s)	28.8 V/m/s (0.73 V/in/s)
Tolerance	± 5%	± 5%
RtBcFn	3,875 Ω Hz	6,000 Ω Hz
Moving mass	16.1 g (0.57 oz)	11.1 g (0.39 oz)
Maximum coil excursion p.p.	4 mm (0.16 in)	4mm (0.16 in)
Physical		
Diameter	25.4 mm (1 in)	25.4 mm (1 in)
Height	36 mm (1.42 in)	36 mm (1.42 in)
Weight	81 g (2.85 oz)	81 g (2.85 oz)
Operating temperature range	-40°C to 100°C (-40°F to +212°F)	-40°C to 100°C (-40°F to +212°F)
Warranty period*	1 year	1 year

(*) Warranty excludes damage caused by high voltage and physical damage to the element case.

All parameters are specified at 20°C in the vertical position unless otherwise stated

SM-11 Geophone

- 30 Hz geophone with high spurious, over 500 Hz, providing wide bandwidth data suitable for up to 1 ms data sampling
- Can be operated in any orientation
- High output through the use of a special magnet and case design
- Rugged mechanical construction, can withstand severe shocks
- 2 year warranty period

The SM-11 geophone is suitable for use in extended frequency, high resolution surveys. It has a natural frequency of 30 Hz and a spurious frequency of over 500 Hz, providing a sensor suitable for use with 1 ms sampling recording systems. The use of a special magnetic circuit makes the output of this geophone higher than normal 30 Hz geophones, ensuring adequate signal strength. The high natural frequency spring design also allows this geophone to be used in any orientation, vertical, horizontal or inverted.

The SM-11 can be installed in the I/O Sensor PE-11 land case.

Typical application: high resolution seismograph reflection studies

Specifications

	SM-11/U-FT
Frequency	
Natural frequency	30 Hz
Tolerance	±5%
Maximum tilt angle for specified Fn	180°
Typical spurious frequency	> 500 Hz
Distortion	
Distortion with 0.7 in/s p.p. coil to case velocity	< 0.2%
Distortion measurement frequency	30 Hz
Maximum tilt angle for distortion specification	180°
Damping	
Open circuit damping	0.55
Open circuit damping tolerance	±5%
Resistance	
Standard coil resistances	360 Ω
Tolerance	±5%
Sensitivity	
Open circuit sensitivity	30 V/m/s (0.75 V/in/s)
Tolerance	±5%
RtBcFn	7,785 ΩHz
Moving mass	9.2 g (0.32 oz)
Maximum coil excursion p.p.	> 1 mm (> 0.04 in)
Physical Characteristics	
Diameter	26.6 mm (1.02 in)
Height	32 mm (1.26 in)
Weight	89 g (3.13 oz)
Operating temperature range	-40°C to 100°C (-40°F to 212°F)
Warranty period*	2 years

(*) Warranty excludes damage caused by high voltage and physical damage to the element case.

All parameters are specified at 20 deg. C in the horizontal position unless otherwise stated

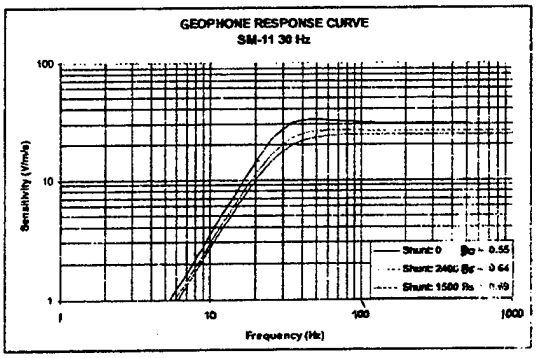

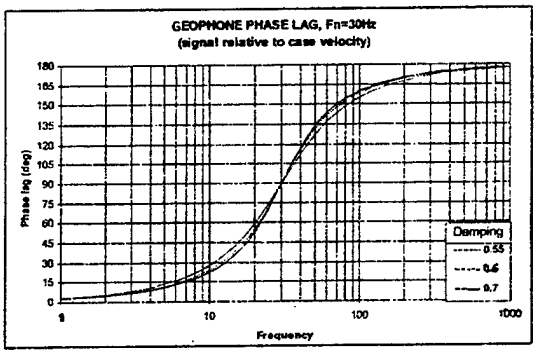

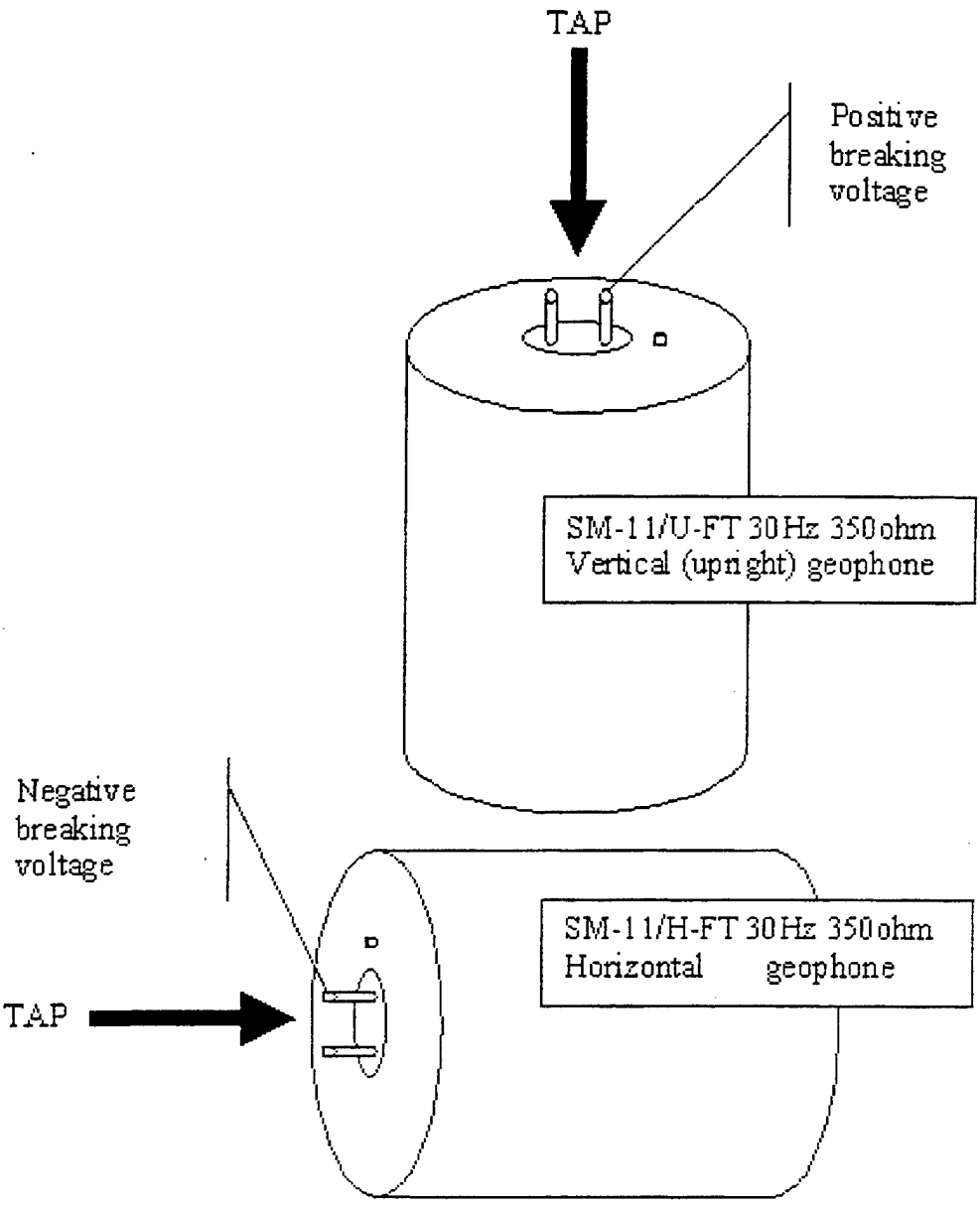
TAP
Positive
breaking
voltage
SM-11/U-FT 30Hz 350ohm
Vertical (upright) geophone
Negative
breaking
voltage
SM-11/H-FT 30Hz 350ohm
Horizontal geophone
TAP

THIS PAGE INTENTIONALLY LEFT BLANK

APPENDIX B. MANUFACTURER SPECIFICATIONS AURA BASS SHAKER

Specifications:	AST-1B-4 Bass Shaker
Frame Size:	4.75" dia. X 2.35" h
Magnet Type:	Ceramic
Power Rating:	Nominal 25 W
Force, Nominal:	10 lbf (44.5 N)
Weight:	2.5 lbs each
Resonance Frequency (fo):	42 Hz
Usable Frequency Range:	20-100 Hz

THIS PAGE INTENTIONALLY LEFT BLANK

LIST OF REFERENCES

1. Department of the Navy, *...From the Sea: Preparing the Naval Service for the 21st Century,* Washington, D.C.: U.S. Government Printing Office, Sep. 1992.
2. Department of the Navy, *Forward...From the Sea,* Washington, D.C.: U.S. Government Printing Office, Sep. 1994.
3. U.S. Marine Corps Headquarters, *Operational Maneuver from the Sea,* Headquarters Marine Corps, Jan. 1996.
4. Hailbig, Capt. Michael T., "Tuzla Team Overcomes Mud, Mines to Help Aircraft Land." [http:// www.af.mil / news/ Dec. 1995 / n19951227_1457.html]. Dec. 1995.
5. Garamone, Jim, "Cohen, Shelton Ask Relief from Land Mine Ban." [http:// www.dtic.mil /afps/ news/ 9805119.html]. May 1998.
6. Gillert, Douglas J., "Korean Economic Woes, Threat from North Concern Cohen." [http:// www.dtic.mil /afps/ news/ 9802023.html]. Feb. 1998.
7. Zamora, George, "Detecting Land Mines." [http:// www.nmt.edu /mainpage/ news/ landmine.html]. Sep. 1997.
8. Miles, Donna, "Confronting the Land Mine Threat." [http:// www.dtic.mil / afps / news / 9806192.html]. June 1998.
9. Dye. D, *High Frequency Sonar Components Of Normal And Hearing Impaired Dolphins*, Master's Thesis, Naval Postgraduate School, Monterey, CA, Sep. 2000.
10. Miles, Donna, "DOD Advances Countermine Technology", [http:// www.dtic.mil / afps / news / 9806193.html]. June 1998.
11. Muir, T.G., Smith, D.E., Wilson, P.S., "Seismo-Acoustic Sonar for Buried Object Detection," Preceedings of the Symposium, *Technology and the Mine Problem*, Naval Postgraduate School, Monterey, CA, Sep. 1995
12. Gaghan, Jr., F.E., *Discrete-Mode Source Development and Testing for New Seismo-Acoustic Sonar*, Master's Thesis, Naval Postgraduate School, Monterey, CA, Mar. 1998.
13. Fitzpatrick, S.M., *Source Development for a Seismo-Acoustic Sonar*, Master's Thesis, Naval Postgraduate School, Monterey, CA, Dec. 1998.
14. Hall, P.W., *Detection and Target-Strength Measurements of Buried Objects Using a Seismo-Acoustic Sonar*, Master's Thesis, Naval Postgraduate School, Monterey, CA, Dec. 1998.
15. Rauch, Dieter, "Seismic Interface Waves in Coastal Waters: A Review", *SACLANT ASW Research Center Report,* SR-42, pp. 9-13, Nov. 1980.

16. Dobrin, M.B., and Savit, C.H., *Introduction to Geophysical Prospecting*, 4th ed., McGraw-Hill Book Company, 1988.

17. Kolsky, H. *Stress Waves in Solids*, pp.1-25, Dover Publications, Inc.,1963

18. Viktorov, I.A., *Rayleigh and Lamb Waves, Physical Theory and Application*, Plenum Press, 1967.

19. Ben-Menahem, A., and Singh, S.J., *Seismic Waves and Sources*, Springer-Verlag, 1981.

20. Richard, F.E., Hall, J.R., Woods, R.D., *Vibrations of Soils and Foundations*, Prentice Hall, Inc, 1970.

21. Zambartas, M., *Introduction to Hidden Markov Models and Their Applications to Classification Problems*, Master's Thesis, Naval Postgraduate School, Monterey, CA, Sep. 1999.

22. Zambartas, M., Fargues, M., "Classification of Mine-Like Objects using Seismo-Acoustic Data", paper presented at the Asilomar Conference on Signals, Systems, and Computers, 33rd, Pacific Grove, California, Oct. 1999.

23. Plagar, W., *Mine Burial in the Surf Zone*, Master's Thesis, Naval Postgraduate School, Monterey, CA, Sep. 2000.

24. U.S. Geographic Survey, *Geographic Reference Image*, U.S. Geographic Survery, 1999.

25. Urick, R.J., *Principles of Underwater Sound for Engineers*, Mcgraw-Hill Book Company, 1967.

26. BBN Systems and Technologies Corporation Technical Memorandum N0. W1068, *Fundamentals of Bistatic Active Sonar,* by Henry Cox, p. 2-6, Jul. 1988.

27. Smith, E. Wilson, P., Bacon, F., Manning, J., Behrens, J., Muir, T. "Measurement and Localization of Interface Wave Reflections from a Buried Target", *Journal Acoustical Society America*, 103(5), Pt. 1, May 1998.

INITIAL DISTRIBUTION LIST

1. Defense Technical Information Center 2
   8725 John J. Kingman Road, Suite 0944
   Ft. Belvoir, VA 22060-6218

2. Dudley Knox Library 2
   Naval Postgraduate School
   411 Dyer Road
   Monterey, CA 93943-5101

3. Commander 1
   PEO Mines
   2531 Jefferson Davis Hwy
   CP6 #920
   Arlington, VA 22242

4. Commander 1
   Expeditionary Warfare, N-75
   Pentagon
   Arlington, VA 22242

5. COMINEWARCOM 1
   325 5th St. SE
   Corpus Christi, TX 78419-5032

6. Commander 1
   Marine Corps Combat Development Command
   Quantico, VA 22134-5027

7. Commander 1
   Marine Corps Systems Command
   Quantico, VA 22134-5027

8. Deputy Chief of Naval Research (ONR) and Commander, ... 1
   USMC Warfighting Laboratory
   Quantico, VA 22134-5027

9. Dr. Douglas Toderoff 1
   Office of Naval Research, Code 322W
   800 N. Quincy St.
   Arlington, VA 22217-5660

10. Dr. Jeffrey Simmen 1
Office of Naval Research, Code 3210A
800 N. Quincy St.
Arlington, VA 22217-5660

11. Dr. Edward Estalot 1
Office of Naval Research, Code 3210A
800 N. Quincy St.
Arlington, VA 22217-5660

12. Dr. Kelly Sherbondy 1
CECOM RDEC NVESD
U.S. Army, Ft. Belvoir, VA 22060-6218

13. Dr. Raymond Lim 1
Coastal Systems Station, Code R22
6703 W. Highway 98
Panama City, Florida 32407-7001

14. Dr. David Tubridy 1
Coastal Systems Station
6703 W. Highway 98
Panama City, Florida 32407-7001

15. Dr. Nickolas P. Chotiros 1
Applied Research Laboratories
University of Texas at Austin
P.O. Box 8029
Austin, TX 78713-8029

16. Dr. Clark Penrod 1
Applied Research Laboratories
University of Texas at Austin
P.O. Box 8029
Austin, TX 78713-8029

17. Dr. Peter Rogers 1
School of Mechanical Engineering
Georgia Institute of Technology
Atlanta, GA 30332

18. Dr. Peter Krumhansel 1
Bolt, Beranek, & Newman, Inc.
Union Station
New London, CT 06320

19. Professor Thomas G. Muir, Code PH/Mu 2
Department of Physics
Naval Postgraduate School
Monterey, CA 93943-5000

20. Professor Steven R. Baker, Code PH/Ba 2
Department of Physics
Naval Postgraduate School
Monterey, CA 93943-5000

21. Professor Monique Fargues, Code ECE/Fa 1
Department of Electrical and Computer Engineering
Naval Postgraduate School
Monterey, CA 93940-5000

22. Professor Anthony Healey, Code ME/He 1
Department of Naval and Mechanical Engineering
Naval Postgraduate School
Monterey, CA 93940-5000

23. COL Eugene T. Daniels Jr. 1
ONR Expeditionary Warfare Technical Division, Code 353
800 N. Quincy St.
Arlington, VA 22217-5660

24. LtCol Mark Miller 1
ONR Expeditionary Warfare Technical Division, Code 353
800 N. Quincy St.
Arlington, VA 22217-5660

25. MAJ Patrick W. Hall 1
3211 Titanic Drive
Stafford, VA 22554-2628

26. CPT Kraig E. Sheetz 1
RD#2 Box 608
Greensburg, PA 15601

27. LT Frederick E. Gaghan 1
846 Central Ave.
New Providence, NJ 07974

28. LT Sean M. Fitzpatrick 1
12362 Caminito Festivo
San Diego, CA 92131

29. Lt Craig Wilgenbush 1
Department of Electrical and Computer Engineering
Naval Postgraduate School
Monterey, CA 93940-5000

30. Mr. Jeremie Guy 1
100 rue des Marmuzots
21000 Dijon
FRANCE

31. Mr. K.C. Pfluger 1
U.S. Marine Corps Representative
Naval Research Laboratory
4555 Overlook Ave. S.W.
Washington, DC 20375

32. Mr. William C. Schneck 1
CECOM RDEC NVESD
U.S. Army, Ft. Belvoir, VA 22060-6218

33. Library 1
Applied Research Laboratories
University of Texas at Austin
P.O. Box 8029
Austin, TX 78713-8029

34. Library, Coastal Systems Station 1
6703 W. Highway 98
Panama City, Florida 32407-7001